3-17-2009

Range Estimation Algorithm Comparison in 3-D Flash LADAR Data

Steven P. Jordan

Range Estimation Algorithm Comparison in 3-D Flash LADAR Data

THESIS

Steven P. Jordan, Captain, USAF

AFIT/GE/ENG/09-22

DEPARTMENT OF THE AIR FORCE
AIR UNIVERSITY

AIR FORCE INSTITUTE OF TECHNOLOGY

Wright-Patterson Air Force Base, Ohio

The views expressed in this thesis are those of the author and do not reflect the official policy or position of the United States Air Force, Department of Defense, or the United States Government.

AFIT/GE/ENG/09-22

Range Estimation Algorithm Comparison in 3-D Flash LADAR Data

THESIS

Presented to the Faculty

Department of Electrical and Computer Engineering

Graduate School of Engineering and Management

Air Force Institute of Technology

Air University

Air Education and Training Command

In Partial Fulfillment of the Requirements for the

Degree of Master of Science in Electrical Engineering

Steven P. Jordan, BSEE

Captain, USAF

March 2009

AFIT/GE/ENG/09-22

Range Estimation Algorithm Comparison in 3-D Flash LADAR Data

Steven P. Jordan, BSEE
Captain, USAF

Approved:

Stephen C. Cain, PhD (Chairman)	3 March 09 Date
Richard K. Martin, PhD (Member)	27 Feb 2009 Date
Richard D. Richmond (Member)	17 March 09 Date

AFIT/GE/ENG/09-22

Abstract

Range estimation algorithms have been applied to Laser Detection and Ranging (LADAR) data to test for accuracy and precision. Data was acquired from Matlab® simulations and an experiment using the Advanced Scientific Concepts 3-D flash LADAR camera. Simulated LADAR data was based on a Gaussian pulse shape model with Poisson noise added. Simulations were performed to test range estimation algorithm performance with respect to waveform position within the range gate. The effectiveness of each algorithm is presented in terms of its average root mean square error and standard deviation in 1000 trials. The measured data experiment examined the effectiveness of an algorithm's ability to determine a range difference between 2 flat surfaces. The algorithms compared for analysis include a peak, maximum likelihood, and matched filter estimator. Various interpolation strategies were implemented in the peak estimator. The matched filter was implemented in the time and frequency domains. A normalized version of the matched filter was also developed and applied to the LADAR data. Three different methods based on averaging were developed to calibrate the pulse width of the reference waveform used in the matched filters and maximum likelihood algorithms.

Simulation results show that a matched filter produces a bias when waveforms are off center, but normalizing waveforms before computing the cross correlation can reduce the average bias from 0.335 meters to 0.124 meters. The maximum likelihood algorithm also produces a bias in shifted waveforms, while the peak estimator maintains a nearly constant level of bias in its measurements due to the effect of shot noise on waveforms. In the measured data sets, normalization did not reduce the bias in measurements because it increased the algorithm's sensitivity to errors in the reference waveform model. The maximum likelihood algorithm's sensitivity to errors in modeling were revealed due to its poor performance in the measured data.

Acknowledgements

Thanks goes out to my research advisor, Dr. Stephen Cain, for guiding my research and offering advice, encouragement, and ideas. Thank you for making yourself available and helping me accomplish something I never thought I'd do. Thank you also to Dr. Richard Martin and Mr. Richard Richmond for serving on my committee and providing the necessary tools and background to support my research.

I'd also like to thank my wonderful wife for always listening and being there for me. Thanks also goes out to Gabe, Larry Hama, my family, and my friends for providing the necessary distractions to stay sane and happy while working.

Steven P. Jordan

Table of Contents

Page

Page

List of Figures

List of Tables

Table Page

List of Symbols

Symbol		Page
$I(r_k)$	Intensity of return pulse	6
r_k	Range sample	6
G	Gain or amplitude of return pulse	6
R	Range to target	6
p_w	Half pulse width of parabolic pulse	6
B	Bias or background noise	6
q	Sensor noise	6
σ_w	Pulse width or standard deviation of Gaussian pulse	7
ρ_t	Reflectivity of target	8
dA	Area of target	8
I_{target}	Intensity reflected from target	8
P_{trans}	Power transmitted	8
θ_t	Beam width	8
P_{target}	Reflected power from target	8
$I_{aperture}$	Intensity at aperture	8
η_{atm}	Atmospheric transmission factor	9
P_{sig}	Power return to receiver	9
D	Diameter	9
η_{sys}	System efficiency factor	9
η_d	Quantum efficiency	9
q	Charge of an electron	9
h	Planck's constant	9
v	Frequency of laser light	9
$d(r_k)$	Model of return pulse data	16
$B(r_k)$	Background energy in individual pixel	16
B_{avg}	Average background energy over 19 samples	16

Symbol		Page
R_{peak}	Range estimated using peak estimator algorithm	21
$f(r_k)$	Reference waveform model	23
τ	Shift value	23
N	Total number of samples	23
C	Simplified cross correlation function	24
R_{mftd}	Range estimated by the matched filter in the time domain	24
R_{gate}	Range gate values	24
$D(w)$	Fourier Transform of data	25
$F(w)$	Fourier Transform of reference waveform model	25
Δf	Original sampling frequency	26
N_1	Number of samples before interpolation	26
Δt_1	Current time between samples	26
Δt_2	Desired time between samples	26
N_2	Number of samples after interpolation	26
$L(R)$	Log likelihood function	28
R_{ML}	Range estimated by maximum likelihood algorithm	29
$\hat{d}(r_k)$	Normalized data	30
$\bar{d}(r_k)$	Mean value of data	31
σ_d	Standard deviation of data waveform	31
$\hat{f}(r_k)$	Normalized version of reference waveform	31
$\bar{f}(r_k)$	Mean value of reference data	31
σ_f	Standard deviation of reference waveform data	31
$\hat{C}_{d,f}(\tau)$	Normalized cross correlation	32
R_{NCTD}	Range estimated by normalized matched filter algorithm	32
$d_n(r)$	Data with timing jitter noise	40
n_{tj}	Timing jitter noise	40
$\Delta D(r)$	Range difference measurment	41

List of Abbreviations

Abbreviation		Page
LADAR	Laser Detection and Ranging	1
ASC	Advanced Scientific Concepts	1
LIDAR	Light Detection and Ranging	4
FOV	Field of View	4
APD	Avalanche Photodiode	4
FPA	Focal Plane Array	4
GPS	Global Positioning System	5
ML	Maximum Likelihood	26
PDF	Probability Density Function	26
PWE	Pulse Width Estimation	33
APE	Averaging Pulses then Estimating	33
EWA	Estimating Widths then Averaging	34
EWNA	Estimating Widths No Averaging	34
AFRL	Air Force Research Laboratory	39
RYJ	Sensors Directorate Electro-Optics Division	39
RMSE	Root Mean Square Error	47
SNR	Signal-to-Noise Ratio	64

Range Estimation Algorithm Comparison in 3-D Flash LADAR Data

I. Introduction

1.1 Problem Statement

Laser Detection and Ranging (LADAR) systems have become an integral part of the technology used by both military and civilian personnel for increasing knowledge of a scene. With an expanding range of applications from target recognition to guidance and navigation, there is no shortage for research and expansion of LADAR technologies.

One fundamental aspect of LADAR is understanding the ability to determine the range to an object based on the detected return pulse reflected off a target. The goal of this research is to understand how different range estimation algorithms can be applied to different scenarios based on waveform shape, size, and position within a respective range gate and which estimation technique delivers the best performance in terms of accuracy, precision, and speed.

1.2 Research Goals

The primary goal of this research is to serve as a catalog comparison of range estimation techniques for the Advanced Scientific Concepts (ASC) 3-D flash LADAR camera system. Several variations on algorithms have been tested in recent years, but there has not been definitive documentation of each technique, nor a side by side comparison of each method under controlled conditions.

This research will also attempt to expand or improve upon existing techniques in order to increase speed and accuracy. New techniques and algorithms discovered during the research process will also be included in the study.

Another goal of the research is to examine the performance of the algorithms under hit mode and sular mode conditions. A description of the camera's operating modes is included in Section 2.6. The effectiveness of a range estimation technique's results in hit mode will be analyzed by observing the range estimation bias and standard deviation as a function of the position of a return pulse waveform within the range gate.

The final outcome of this research will produce one proven method for determining the range of a target using the 3-D flash LADAR camera. It will also be feasible to describe when each algorithm will be preferred over other algorithms based on the noise, camera modes, or other distinguishing factors.

1.3 Scope of Research

The research will be performed on data that is simulated via Matlab® and on data produced from the ASC 3-D flash LADAR camera. While some aspects of the algorithms will be universal to any laser radar system, the final product designed will be made with the intention of its use under the ASC 3-D flash LADAR camera system. The hit mode operation study will be specific to the ASC camera system and would only pertain to other systems that may operate with a similar threshold trigger technique.

Noise introduced and simulated in the data will be based on the ASC camera system. Again, some noise sources are universal to LADAR principles, but some may be specific to the camera system such as specific dark current noise levels used during measured data observations.

While this research is dedicated to documenting and examining effectiveness of the range estimation algorithms, some additional sources of noise and error may be discovered along the way. These noise sources will be documented when observed, but the optimal solution for their mitigation may not be covered in the scope of this research.

1.4 Document Overview

The thesis document begins in Chapter 1 with an introduction of the problem and a description of the research performed. Chapter 2 continues with appropriate background information on past work pertaining to the ASC 3-D flash LADAR camera and the incorporation of LADAR systems for military applications. Chapter 2 also contains a history of several range estimation techniques that have previously been applied to LADAR data. Chapter 3 describes the new developments related to range estimation techniques. The methodology for performing the experiments in both simulated and measured data is included in Chapter 4. Chapter 5 presents the results of the experiments while Chapter 6 contains the final conclusions and suggestions for future research in related areas.

II. Background

Chapter II contains information within the scope of the research that will provide a suitable background for the reader. The background chapter contains information on applications of laser radar, range equation development, and range estimation theory.

2.1 Laser Radar Development

Traditional microwave radar systems operate in a variety of wavelengths within the electromagnetic spectrum. Depending on the application, operation wavelengths can vary from 100 m (High Frequency Band) to several millimeters (Wide Band) [6]. In contrast to traditional microwave radar, laser radar operates on a much shorter wavelength of the electromagnetic spectrum typically ranging from 10.6 μm to 0.4 μm [6]. Light Detection and Ranging (LIDAR) systems are designed around an electro-optical device that transmits an outgoing pulse in the optical electromagnetic spectrum. Receiver optics collect the return pulse data and digitize the signal for future use in post processing algorithms. Data can be interpreted to analyze the intensity, time of flight, and range information. LADAR systems are a specific category of LIDAR where the optical transmission source is a laser [6]. Early LADAR systems for 3-D imaging were designed around scanning systems where a mechanical device moved the beam across a target area in order to collect enough information to build a scene or image of the illuminated area. By 1996, scannerless systems were developed that allowed an area with a larger field of view (FOV) to be illuminated in a single shot [10]. Scannerless systems, now often referred to as flash systems, benefit from less moving parts which can translate to reduced cost, smaller hardware footprint, and improved reliability [10, 13]. Avalanche Photodiode (APD) arrays are now the customary technology used in a Focal Plane Array (FPA) fashion to collect the return pulse information and form pixels of data that can be analyzed using signal processing techniques to determine the range to each pixel [13].

2.2 Laser Radar Applications

LADAR technology has many diverse roles in both civilian and military applications including remote sensing, target recognition and identification, and guidance or navigation enhancement [6]. The need for 3-D imaging systems for military purposes comes from an evolution of warfare that demands precision guided weapons, increased situational awareness, quicker reaction times, and reduced collateral damage. LADAR imaging can provide decision makers the necessary tools to meet these demands both on and off the battlefield. LADAR applications extend from land based applications to both aerial and maritime techniques [3]. One of the most favored applications for LADAR involves repeatedly illuminating an area obscured by foliage or netting and collecting the return data in order to form an image of what is hidden beneath [13]. There is also an emerging potential to use LADAR systems to allow helicopter pilots see through dust or sand clouds caused by spinning rotors at low altitudes as presented in [12]. As the demand for unmanned vehicles increases, LADAR systems can be incorporated to provide vision, security, and collision avoidance as proven in past trials with robotics [9]. Existing technology, such as the Global Positioning System (GPS), could potentially be fused with LADAR data to further enhance the information available to decision makers and operators and provide back up navigational controls. By accurately developing LADAR technology and corresponding signal processing techniques required for analyzing the data, one could improve target recognition, feature tracking, and other aspects of 3-D imaging applications.

2.3 Laser Radar Waveform Models

In order to accurately simulate LADAR return pulse data, it is imperative to have an accurate model of the waveforms that are received by the detector. A thorough and robust development of the waveform model will deliver more accurate results in simulations. A well developed model will also deliver more accurate range estimates for algorithms that depend on a reference waveform such as the matched filter and maximum likelihood algorithms discussed in Section 2.8. In general, the return pulse

is formed as a function of the convolution of the outgoing laser pulse and the surface of the target. The basic shape of the original laser pulse, with the addition of noise sources, should still be maintained. Three common methods exist for modeling the return pulse shapes.

2.3.1 Parabolic Waveform Model. The simplest model is that of an inverse parabolic waveform. This model has been explored and tested in both [1] and [2]. As adapted from [2] the inverse parabolic waveform is shown by

$$I(r_k) = G \times \left(1 - \frac{(R - r_k)^2}{(p_w)^2}\right) rect\left(\frac{(R - r_k)}{2p_w}\right) + B + q \tag{2.1}$$

where $I(r_k)$ is the intensity of the pulse in photoelectrons at range sample r_k, G is the gain or amplitude of the pulse, R is the range to the target, p_w is the half pulse width of the target in range units. B represents the bias or background noise of the signal in terms of photoelectrons, and q represents the noise of the sensor added to the signal. As shown in [5] the rectangle function is defined as

$$rect(x) = \begin{cases} 1 & \text{if } |x| < \frac{1}{2} \\ 0 & \text{else} \end{cases} \tag{2.2}$$

and is used to limit the waveform to positive values.

Figure 2.1 illustrates the idea that the inverse parabolic can provide a suitable fit to a measured return pulse from the ASC 3-D flash LADAR.

2.3.2 Gaussian Waveform Model. Another option for the waveform model incorporates a Gaussian shaped pulse as the basis for the waveform model. The width of the Gaussian pulse can be adjusted by using different values for the standard deviation. Based on previous observations of measured data, the waveforms used in simulations will be modeled as a Gaussian pulse where the intensity, $I(r_k)$, in

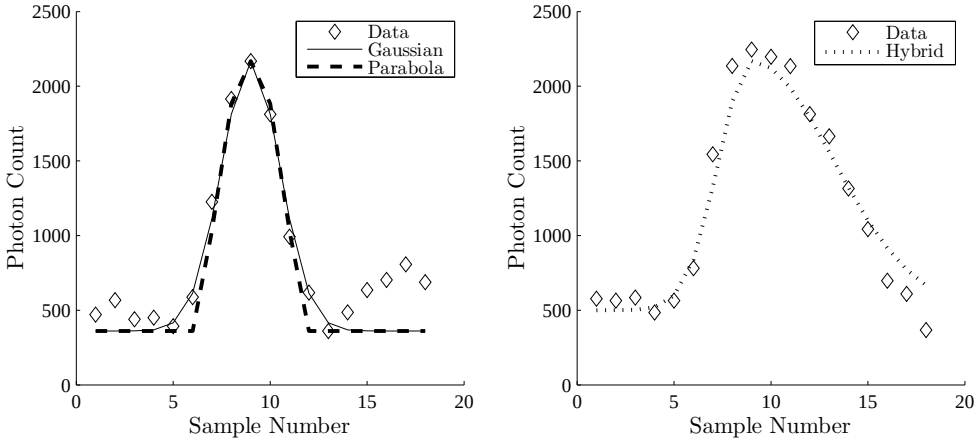

(a) Parabolic and Gaussian Waveform Models

(b) Hybrid Waveform Model

Figure 2.1: a) Symetric LADAR data with comparison to parabolic and Gaussian waveform models. b) Skewed waveform data with a hybrid model used to fit data. First half of pulse is using a 2 ns pulse width while the second half of the pulse is using a 5 ns pulse width.

photoelectrons of each sample k is calculated using the equation

$$I(r_k) = \frac{G}{\sqrt{2\pi}\sigma_w} e^{\frac{-(r_k - R)^2}{2\sigma_w^2}} + B + q \tag{2.3}$$

where σ_w is the pulse width or standard deviation, G is the amplitude, r_k is the range for a given sample k in meters, and R is the range to the target. B and q again represent the bias and noise added to the signal. Reference Figure 2.1 to observe the fit the Gaussian waveform model with measured data.

2.3.3 Hybrid Waveform Model. Another model for simulation and building a reference waveform involves the design of a hybrid waveform model. This more complex method involves two combinations of either the parabola and Gaussian waveform models with different widths for each half to yield a model that is better suited to fit the measured return pulse from the ASC 3-D flash LADAR. Figure 2.1 shows the comparative fit of the hybrid and measured data. The hybrid waveform model is best used for waveforms that appear to be skewed or asymmetric.

2.4 Laser Radar Range Equation

Accurate range estimation techniques require a thorough understanding of the principles behind the propagation of the laser pulses reflected off the target in question. A model for the range equation of the return signal's intensity is presented in [6] and will be followed for the purposes of this research.

To obtain the correct power in each sample during simulations, each sample is propagated down range and the intensity of the return sample is computed using the range equation described in [6]. The range equation has a direct dependence on the area of the target which affects the cross section of a target. The cross section of the target is dependent upon whether the target is a point source, Lambertian, or other type. In all simulations and experiments used for this research the target was a Lambertian diffuse target where the cross section, σ, is

$$\sigma = 4\rho_t dA \tag{2.4}$$

where ρ_t is the reflectivity of the target and dA is the area of the target. The intensity of the energy reflected from the target, I_{target}, is a function of the cross section and the intensity of the laser illuminating the target shown by

$$I_{target} = \frac{P_{trans}}{4\pi R^2} \times \frac{4\pi}{\theta_t^2} \tag{2.5}$$

where P_{trans} is the power transmitted, R is the range to the target, and θ_t is the beam width. The power reflected from the target, P_{target}, is now given by

$$P_{target} = \sigma I_{target} \tag{2.6}$$

and can be used to find the intensity at the aperture, $I_{aperture}$, of the receiver using

$$I_{aperture} = \frac{\eta_{atm} P_{target}}{4\pi R^2} \tag{2.7}$$

where η_{atm} is the atmospheric transmission factor. The intensity at the aperture is next used to calculate the power returned to the receiver, P_{sig}, via

$$P_{sig} = \frac{I_{aperture}\eta_{sys}\pi D^2}{4} \tag{2.8}$$

with the assumption that the aperture is circular and D is the diameter in meters. The system efficiency factor, η_{sys} is the transmission efficiency of the receiver multiplied by the efficiency of the detector.

The final end to end range equation used to measure each sample in the waveform is

$$P_{sig} = \frac{P_{trans}\eta_{sys}\sigma\eta_{atm}D^2}{16\theta_t^2 R^4} \tag{2.9}$$

and is converted to photoelectrons by using

$$i_{sig} = \frac{\eta_d q P_{sig} G}{hv} \tag{2.10}$$

where η_d is the quantum efficiency, q is the charge of an electron, G is the gain of the LADAR system, h is Planck's constant, and v is the frequency of the laser light.

2.5 Noise Sources in LADAR data

There are several sources of noise in the LADAR data that can lead to errors in range measurements. This section will describe natural sources of noise that can occur in the data. Sources of noise or error that are directly related to the algorithm processing will be described in the respective section for each algorithm.

2.5.1 Shot Noise. Shot noise is used to account for errors in measurements as a signal reaches the detector and is modeled via a Poisson distribution [6]. Shot noise is related to the strength of the return signal and causes fluctuations in the intensity measurements that can shift the peak of a waveform from its true location.

Figure 2.2 shows the plot of a simulated signal without shot noise and one with shot noise added that has caused a shift in the location of the peak sample.

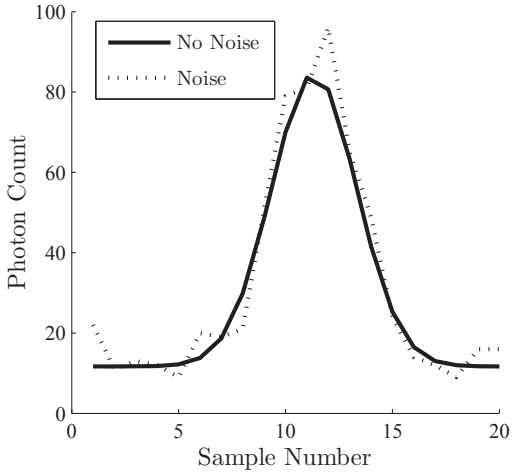

Figure 2.2: Peak is easily shifted with addition of shot noise simulated via a Poisson distribution

2.5.2 Background Noise. Because the sensor records all light levels that enter the detector, background or ambient light levels can have an effect on the intensity of the return signal [6]. The background light levels are added as an averaged bias term that if known, could be subtracted from the data based on the waveform models previously described. The background for a data collection scenario can be obtained by measuring data received by the optics without actually firing the laser pulse. The background intensity during a data capture is shown in Figure 2.3. Light levels can fluctuate between laser shots so this calibration step would need to be performed for each data collection.

2.5.3 Dark Current. Dark current is false positive readings of electrons by the detector that can add noise to the signal [6]. All electro-optic sensors are subject to dark current. Current leakage varies from system to system based on the internal physics and temperature. The dark current of the system can be estimated by measuring return data when the system's receiver optics are covered. The average

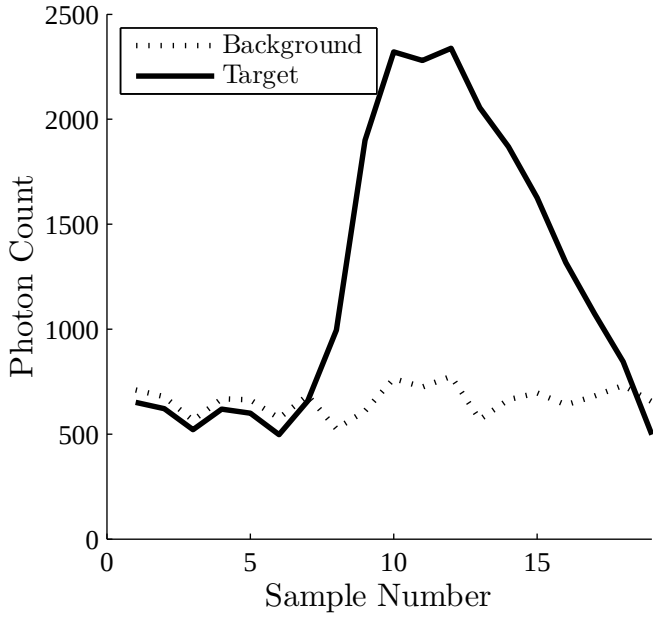

Figure 2.3: Example of background radiation noise compared to signal reflected from target in 3-D flash LADAR camera data

values for a dark current measurement in the ASC 3-D flash LADAR camera have been obtained and can be used to remove dark current bias from the measured data. If dark current values are used they could be included into the overall bias (B) term that includes the background noise. Figure 2.4 illustrates the capture of dark current levels obtained by covering the lens and recording the waveforms. The data was obtained while the camera was in hit mode, so the spike in levels is an anomaly caused by the threshold trigger. Only samples 7-19 would be averaged to obtained the value of the dark current intensity.

2.5.4 Timing Jitter. Timing jitter is another source of noise caused by small fluctuations in the internal clock of the system. Very small changes in timing can cause changes in the time the pulse is received and can lead to errors in range measurements. A method for mitigating the errors caused by timing jitter in the measured data experiment is presented in Section 4.3.

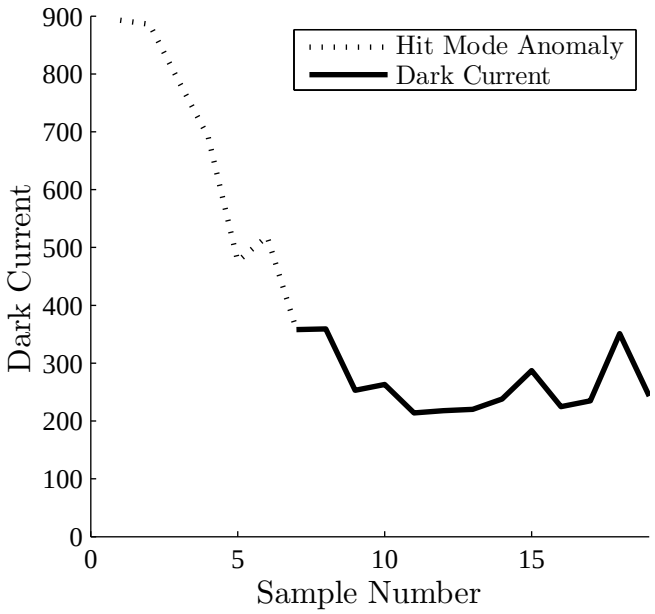

Figure 2.4: Dark current readings from ASC 3-D flash LADAR camera. Spike in first 7 samples is anomaly caused by use of hit mode. Samples have been sorted and marker slice was removed. Final 12 samples would be averaged to obtain an indication of dark current levels in camera system.

2.6 ASC Camera Description

The ASC 3-D flash LADAR camera operates by emitting a laser pulse which is reflected off a target. The reflected energy is processed by the camera's receiver optics. Data is digitized from the optical sensors and transferred to a computer for further processing of the data. The receiver is built around an array of 128 x 128 APDs. The sampling rate of the system is 420 MHz. The memory storage capacity allows for 20 samples to be collected and stored in hard memory. Each sample represents a distance of approximately 36 cm, so the 20 samples collectively allow for a range gate that is slightly over 7.1 meters. However, one sample serves as a marker slice which is removed from the data and stands as a reference for range measurements. This 19 sample set of data builds a usable range gate with a depth of about 6.8 meters. The ASC 3-D flash LADAR camera has the ability to operate in two different modes, sular and hit mode. Hit mode may also be referred to as stop mode in some documentation [11].

2.6.1 Sular Mode Description. In sular mode, the user is allowed to specify a range gate with the depth previously described. Only buffered return pulse data that falls within the specified range gate is stored to form the 20 samples returned to the user for post processing. When the approximate or exact range to the target is known, sular mode is a suitable option to ensure that waveforms are properly captured by the system. However, if the range to the target is unknown or if there is a question of whether or not a target is present, hit mode may serve as a more appropriate choice.

2.6.2 Hit Mode Description. There are conflicting views on the hit mode operations in the ASC 3-D flash LADAR camera. Based on previous camera designs, it was believed that hit mode operations performed based on a user defined threshold in terms of photoelectron counts. Return pulse data is buffered through the system until the threshold of photoelectrons is reached [11]. When the threshold is crossed, 8 samples before the threshold are stored, and 12 samples after the threshold are also stored. Again, this presents the 20 samples used for range calculations. 1 sample serves as a marker slice and is removed from the set doing post processing. In order to reference the waveforms of each pixel properly and build the 128 x 128 different range gates, a 128 x 128 array is stored in the camera's memory that contains the range at which the threshold was crossed for each pixel of data. This is referred to as the hit mode buffer and allows the system to build a separate range gate for each of the 128 x 128 waveforms captured by the system.

Upon further examination of hit mode operations in the newer camera used to collect data for this research, it appears that the previous hit mode operation assumptions are not correct or do not hold true for the new camera system. The 128 x 128 hit mode buffer did not contain values that could sensibly be range measurements to the threshold crossing. Every other row of values contains zeros, which leads to the assumption there is most likely an error in the camera's system when creating the hit mode buffer. For non zero values, it would appear that they represent a marker that dictates which range gate the corresponding waveform would use. Due to the current

errors in the hit mode buffer, only about half the pixels collected in hit mode can be properly used with the range estimation algorithms. After determining the proper range gate to match to the waveforms, they would not be processed any differently from sular mode data. Because of the complications associated with the new cameras hit mode buffer, all the measured data analyzed when comparing the performance of the range estimation algorithms was collected in sular mode.

2.7 Gain Variation in the ASC 3-D flash LADAR System

It has been shown that the gain of the ASC 3-D flash LADAR system used in previous research is not constant as expected, but varies nonlinearly with respect to time [11]. As presented in [7] and [11], the gain of the APD array can fluctuate depending on the internal voltage regulator and current distribution. Return pulses from the LADAR camera would ideally be the same shape and size when reflected from the same target, but through experimentation described in [7] and [11] it has been shown the waveforms fluctuate as seen in Figure 2.5. The waveforms in Figure 2.5 are the collected return signals when the target was a 155 cm x 155 cm square plywood board placed approximately 70 meters from the receiver and perpendicular to the line of sight.

As shown in Figure 2.5 the fluctuation in gain causes the shape of the return pulses to change. The shape of waveforms can become skewed or warped which makes it impractical to create an accurate waveform model based on the skewed waveforms [7]. The lack of a consistent shape that can be easily modeled can mislead certain range algorithms such as the matched filter technique described in Section 2.8.2. Similar to the effect of shot noise, gain variation could possibly shift the peak of a waveform by several samples, which could lead to errors in range measurements when using certain range estimation techniques. Although it was not tested in the scope of this research, it is possible that algorithms such as a leading edge detector may still properly process the unequalized signals.

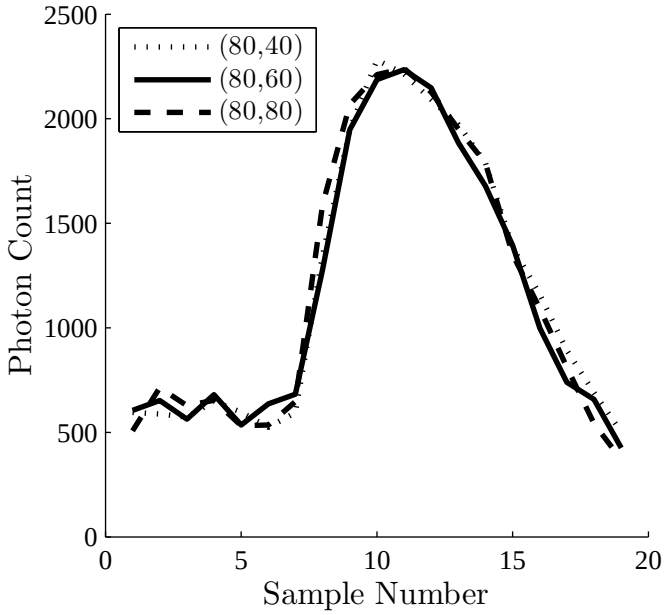

Figure 2.5: Unequalized return pulses from a target approximately 70 meters from receiver and perpendicular to line of sight. Pulses are not symmetric, it appears the second half of the pulses are wider than the first half.

In order to accurately compare the performance of the range estimation algorithms and design a model for the waveforms, the gain variation should be taken into account and corrected before further steps are performed.

One area of concern, however, is the effect of the gain variation when the camera is operating in hit mode. In hit mode the APDs operate independently and each could be firing at different times based on the threshold set by the operator. In this situation, some of the critical assumptions and calculations based on the background levels and relationships will not necessarily hold true. The current draw that causes the gain to fluctuate will not be as strong if the individual APDs are not operating at the same time. Section 2.7.1 will describe in detail the method proposed in [7] for reducing the effects of gain variation on range estimation error.

2.7.1 Estimation and Equalization of Gain Variation. In this section, a technique for estimating the gain variation is presented. The application of the equalization technique is based on the findings of [7] and [11]. Unless otherwise noted, all

equations and references for calculating the gain are under the assumption that the camera is operating in sular mode.

The variation in gain is a direct result of the change in load during the time of data collection when the voltage regulator cannot maintain a constant output [11]. As each sample is taken, the responsiveness of the APD will vary and the gain will fluctuate. As seen in Figure 2.6, the background signal power in a non-target pixel appears constant and then drops significantly at about sample 6 or 7 to coincide with the the first reception of return pulses reflected from the target. In theory, the background light levels observed in pixels that do not contain target information should remain constant. The relationship between the background power and gain given in [7] is

$$i_B(t) = \frac{Gq\eta_q}{hv} P_B \tag{2.11}$$

where G is the gain, q is the charge of an electron, η_q is the quantum efficiency, h is Planck's constant, and v is the frequency of the laser light. To evaluate the gain, the following equation for the model of data, $d(r_k)$, is

$$d(r_k) = G(r_k)\frac{B(r_k)}{B_{avg}} \tag{2.12}$$

where $G(r_k)$ is the gain for sample r_k, and $\frac{B(r_k)}{B_{avg}}$ is the ratio of background in an individual pixel, $B(r_k)$, to the average background value in the pixel over the 19 samples, B_{avg} [7]. If this equation is rearranged in order to solve for the gain, $G(r_k)$, then it would appear as

$$G(r_k) = d(r_k)\frac{B_{avg}}{B(r_k)} \tag{2.13}$$

The data, $d(r_k)$, has already been acquired and the average background values, B_{avg}, can also be calculated from the previous collection of background noise. To estimate the background in the actual data that is affected by the gain, $B(r_k)$, a cluster of

pixels that did not contain any target data during a shot that included a target in the scene was used as the $B(r_k)$ values. These target free pixels were pixels that while illuminated by the laser did not receive any return pulse data. In the data set used for the gain variation studies these pixels can generally be found in the upper right or upper left corner of the scene. The illuminated scene created by the return pulse data can be seen in Figure 2.7. The background readings would be affected by the gain the same as the other pixels. The average background over the same pixels was taken from a background data capture that was recorded separately as seen in Figure 2.3. The resulting value was used as an estimate of the gain. This method creates an array of gain values that is a function of each sample. An example of the estimated average gain value for 19 samples when the target was perpendicular to the line of sight is shown in Figure 2.8.

Equalization of the data is accomplished by dividing the measured data waveforms by the estimated gain waveform on a sample by sample basis. Figure 2.9 shows the results of applying the equalization method to the raw waveforms. The leading edge of the waveforms is much smoother, but the trailing edge is still somewhat distorted. It can also be seen that the equalized waveforms allow the sample's intensities to continue to climb upward in value, while in the unequalized waveforms they are cut short before actually reaching the true location of the target sample. Waveforms still appear to be a combination of two pulse widths that would benefit from a hybrid waveform model.

In [7] it is shown that the gain equalization technique does not eliminate all of the error in range measurements, but does reduce the error. Further experimentation is necessary before a strong conclusion can be made regarding the performance of the gain estimation technique.

2.7.2 Additional Notes on Gain Variation. The data collected and used during this research was gathered with a newer version of the ASC 3-D flash LADAR camera. While the new camera still has some characteristics of the other cameras and

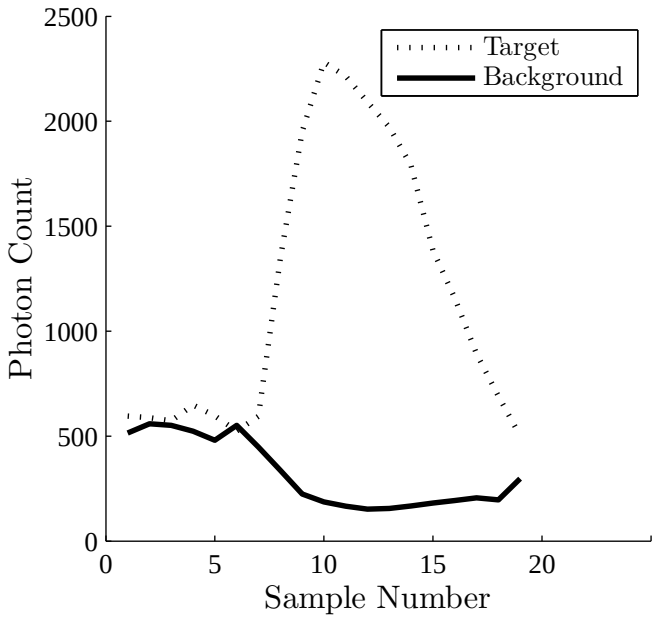

Figure 2.6: Unequalized return pulse in pixel that contains target data compared to an averaged background pixel that does not contain target data. Note the drop in background level that corresponds to the return of the signal reflected off target.

operates in the same fashion, it may be difficult to compare the data and equalization technique of the older camera systems to the newer version. Also, a new technique for eliminating gain variation involving optical filters has been implemented for the purpose of this research. This method will be described in Section 3.1. Because of the apparent lack of gain variation in the new camera and optical filter technique employed, the gain estimation technique described in [7] was not applied to the data used in the range estimation experiments conducted during the scope of this research.

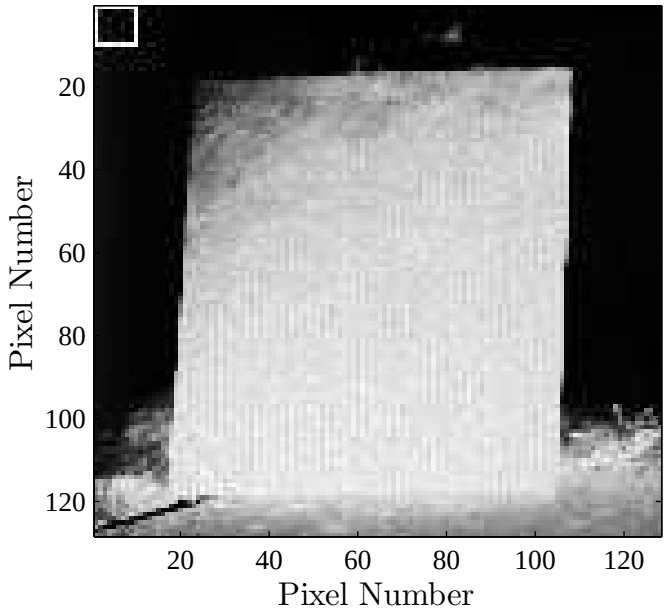

Figure 2.7: Image of scene formed from LADAR intensity data viewed at sample 10. Target is about 70 meters from receiver and normal to line of sight. White square indicates region of scene used to compute background levels in target scene for gain estimation.

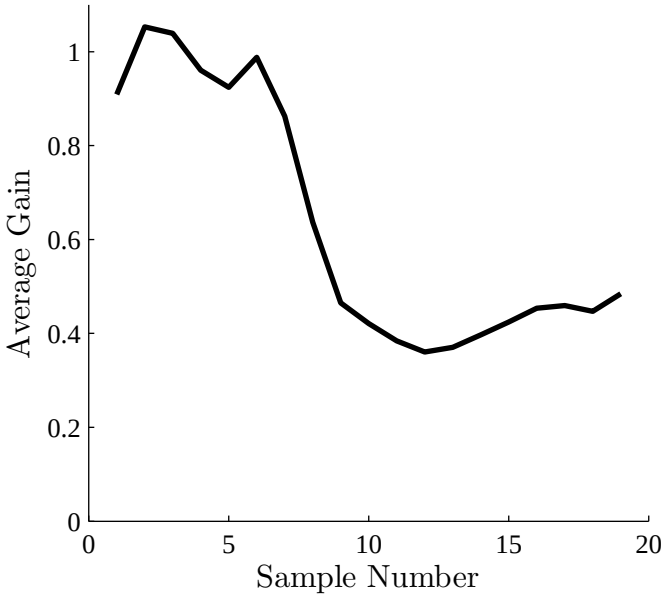

Figure 2.8: Average gain values when target was normal to line of sight. The gain drops significantly at the samples that correspond to the first return pulses from the target.

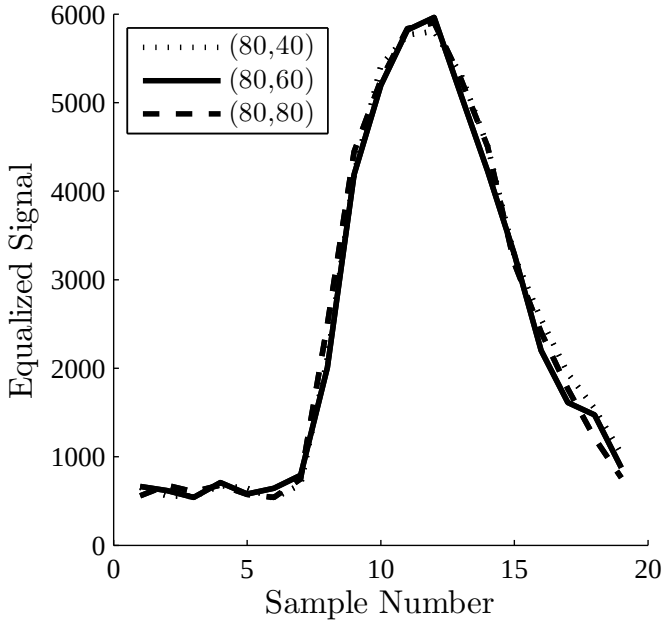

Figure 2.9: Equalized waveforms from the same pixels shown in Figure 2.5.

2.8 Range Estimation Theory

This section will detail current range estimation techniques used in processing LADAR data and provide a derivation or description of each.

2.8.1 Peak Estimation. One of the simplest methods of estimating the range of a return pulse from a LADAR system is the peak estimator. Based on the creation of the waveforms, the largest power of the return sample will theoretically coincide with the sample corresponding to the target range. A critical element of using the peak estimator is having a waveform that includes the true peak of the return pulse. The peak of the received waveform is recorded, and the corresponding range value from that particular sample is chosen as the range estimate. As shown in Section 5.2, the peak estimator algorithm is highly effective in simulations when there is no noise present, but in realistic conditions with the presence of shot noise the peak estimator can easily be misled as illustrated by Figure 2.2. The peak estimator can be described by the equation

$$R_{peak} = \arg\max_{r_k} d(r_k) \tag{2.14}$$

where $d(r_k)$ is the waveform currently used for range estimation. R_{peak} is the range value returned by the peak estimator. To achieve sub-sample range estimations, the waveform can be interpolated using various strategies before searching for the peak. However, in the presence of noise, interpolation could lead to more error in range estimation. Figure 2.10 shows how interpolation can change the data used in the peak estimator. The results in Chapter V will show the benefits of an accurate interpolation strategy when using the peak estimator.

2.8.2 Matched Filter. The matched filter evolves from the idea of using a shifting reference model waveform to cross correlate with the data waveform. The shifted waveform with the highest correlation is used to determine the correct range estimate. It is essential to have an accurate model of the waveform when using a

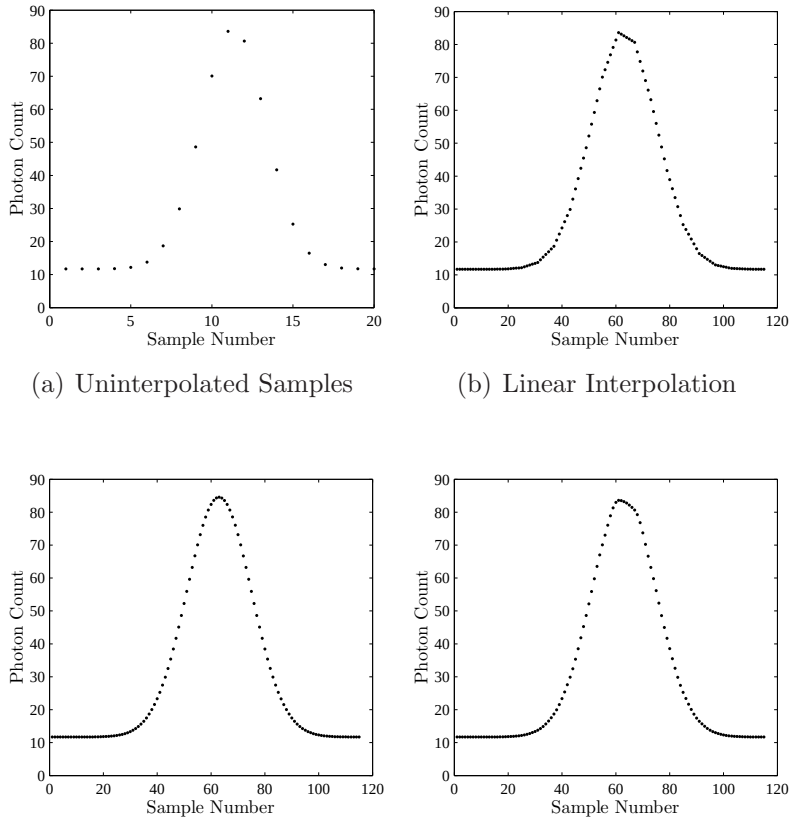

(a) Uninterpolated Samples (b) Linear Interpolation

(c) Cubic Spline Interpolation (d) Shape Preserving Cubic Interpolation

Figure 2.10: a) Simulated LADAR pulse with no interpolation between two samples. b) Linear interpolation used to create additional samples. c) Cubic Spline Interpolation. d) Shape preserving (of original sampled waveform) cubic interpolation.

matched filter, particularly when determining the width of the waveform. A discussion of the sensitivity of the range estimates with respect to the shape and width of the reference model waveform is presented in Chapter V. There are several variations on the matched filter algorithms. The largest variation depends on whether or not the algorithm is implemented in the time or frequency domain. Both methods were used in the scope of this research and are presented in the following sections.

2.8.2.1 Time Domain Correlation. The matched filter is implemented by comparing the data waveform to a reference waveform using a cross correlation technique. In [8] this is shown in two dimensions as a measure of distance between

the two functions described by

$$d^2_{f,t}(u,v) = \sum_{x,y}[f(x,y) - t(x-u, y-v)]^2 \tag{2.15}$$

which can be simplified to one dimension for application to the LADAR waveforms. In one dimension this is shown as

$$d^2_{f,t}(u) = \sum_{x}[f(x) - t(x-u)]^2 \tag{2.16}$$

where a change in variable nomenclature leads to

$$c^2_{d,f}(\tau) = \sum_{k=1}^{N}[d(r_k) - f(r_k - \tau)]^2 \tag{2.17}$$

where $c^2_{d,f}(\tau)$ is the correlation value between the two functions $d(r_k)$ and $f(r_k)$ at a shift value of τ. $d(r_k)$ is the LADAR return pulse data waveform at range sample r_k and $f(r_k)$ is the reference waveform based off of a predetermined model at range sample r_k. The reference waveform is created such that the center or peak value is at the shift value of τ. N is the total number samples in the data waveform. The next step in evaluating the cross correlation is expanding the terms that are a function of the square value. This leads to the equation

$$c^2_{d,f}(\tau) = \sum_{k=1}^{N}[d^2(r_k) - 2d(r_k)f(r_k - \tau) + f^2(r_k - \tau)] \tag{2.18}$$

which can be examined to note that two of the terms, $d^2(r_k)$ and $f^2(r_k - \tau)$ would remain constant after passing through the summation process. Terms that do not change as a function of τ will be removed from the equation because they do not affect the location of maxima and minima points. This simplification step leaves

$$c^2_{d,f}(\tau) = \sum_{k=1}^{N}[-2d(r_k)f(r_k - \tau)] \tag{2.19}$$

which can also be simplified to remove the negative and scalar factors that do not have any effect on changes with respect to τ. This final expression is shown as

$$C_{d,f}(\tau) = \sum_{k=1}^{N} [d(r_k) f(r_k - \tau)] \tag{2.20}$$

which describes the cross correlation, C, of $d(r_k)$ and $f(r_k)$ with respect to the shift value of τ.

The reference waveform, $f(r_k)$, is generated using either the Gaussian, inverse parabola, hybrid, or other model with a peak at different locations corresponding to the guess at the range of the target (τ). The data waveform and the reference waveform samples are individually multiplied by one another and the resulting products summed to form a correlation value for that particular shift. The range estimated by the matched filter in the time domain, R_{mftd}, corresponds to the value of τ that maximizes the correlation, $C(\tau)$ shown by

$$R_{mftd} = R_{gate} \left(\arg \max_{\tau} C(\tau) \right) \tag{2.21}$$

where R_{gate} is the range gate of all potential range values tested by the shifting reference wave. The correlation process in the time domain is illustrated in Figure 2.11.

In [8] it is mentioned that when two signals with energies that can vary with position are used in the matched filter technique, the algorithm will fail. This is illustrated in Section 5.2 where it is shown that there is a bias in the algorithm when the data waveforms are not centered in the range gate. A method to reduce the bias by normalizing the energy of the signals is proposed in Section 3.2.

2.8.2.2 Frequency Domain Correlation. The matched filter technique can also be implemented in the frequency domain by taking advantage of the correlation property of the Fourier Transform described in [4]. Given the Fourier Transform

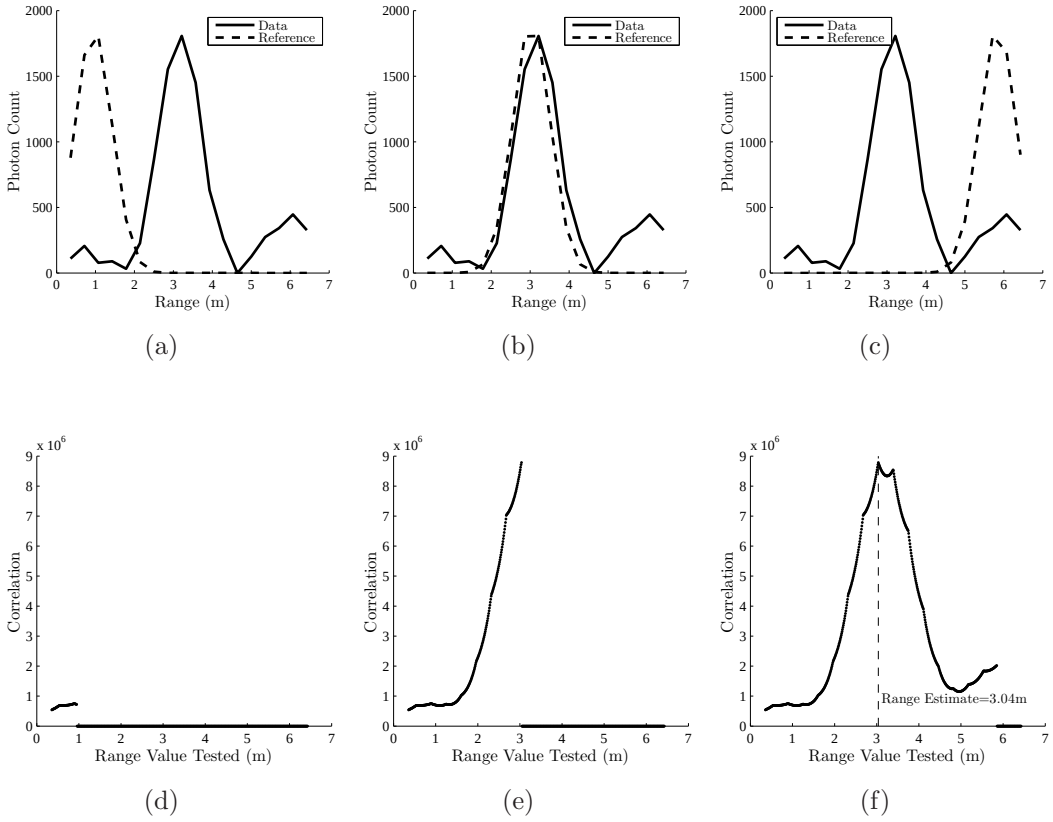

Figure 2.11: Figures a)-c) illustrate the reference waveform as it shifts from left to right across the range gate. Figures d)-e) illustrate the correlation value as the reference waveform shifts position.

of the data is $D(w)$ and the Fourier Transform of the reference waveform is $F(w)$ then

$$\mathscr{F}\{C(\tau)\} = \mathscr{F}\{\sum_{n=0}^{N-1} d(r_k) f(r_k - \tau)\} \tag{2.22}$$

which can be approximated as

$$\mathscr{F}\{C(\tau)\} = D(\omega)F(\omega) \tag{2.23}$$

From here, the range is found by finding the maximum value of the function $\mathscr{F}\{C(\tau)\}$ and finding its corresponding range sample. This can lead to a much faster computation as the number of operations is drastically reduced. Sub sample interpolation is achieved by zero padding both the data and reference waveform in the frequency

domain before multiplication. The desired level of interpolation is achieved by first finding the current sampling frequency, Δf, by using

$$\Delta f = \frac{1}{N_1 \Delta t_1} \tag{2.24}$$

where N_1 is the current number of samples and Δt_1 is the current time between samples. If the desired level of time between samples is Δt_2 then the number of samples to be added by zero padding, N_2, is found by the equation

$$N_2 = \frac{1}{\Delta t_2 \Delta f} = N_1 \cdot \frac{\Delta t_1}{\Delta t_2} \tag{2.25}$$

N_2 can now be used with N_1 to determine the appropriate number of zeros needed to add to either side of the waveform. If a desired number of samples is required instead of the preset sampling distance, interpolation can be accomplished in the same manner by solving for the appropriate variable. However, it would not be possible to properly normalize a waveform as described in Section 3.2 if this method were used.

2.8.3 Maximum Likelihood. The maximum likelihood (ML) estimator is derived by determining the probability density function (PDF) of the data at one range sample instance, r_k. In [2] it is determined that the largest source of noise would come from the shot noise in the signal. Because shot noise is modeled as Poisson, the PDF for one sample is

$$P[D(r_k) = d(r_k)] = \frac{I(r_k)^{d(r_k)} e^{-I(r_k)}}{d(r_k)!} \tag{2.26}$$

where $I(r_k)$ is the data generated by one of the waveform models described in Section 2.3. The data is designated by $d(r_k)$. Due to the assumed independence between the noisy samples, the joint PDF is the product of the individual PDFs shown by

$$P[D(r_k) = d(r_k) \forall k \in [1, N]] = \prod_{k=1}^{N} \frac{I(r_k)^{d(r_k)} e^{-I(r_k)}}{d(r_k)!} \tag{2.27}$$

To simplify the process of maximizing the probability, the maximum of the log of Equation (2.27) will be found. The first step is accomplished by taking the natural log of both sides shown by

$$ln\left(P\left[D(r_k) = d(r_k) \forall k \in [1, N]\right]\right) = ln\left(\prod_{k=1}^{N} \frac{I(r_k)^{d(r_k)} e^{-I(r_k)}}{d(r_k)!}\right) \tag{2.28}$$

which is simplified to

$$L = \sum_{k=1}^{N} ln\left(\frac{I(r_k)^{d(r_k)} e^{-I(r_k)}}{d(r_k)!}\right) \tag{2.29}$$

This expression can further be simplified to

$$L = \sum_{k=1}^{N} ln\left(I(r_k)^{d(r_k)} e^{-I(r_k)}\right) - ln\left(d(r_k)!\right) \tag{2.30}$$

and

$$L = \sum_{k=1}^{N} ln\left(I(r_k)^{d(r_k)}\right) + ln\left(e^{-I(r_k)}\right) - ln\left(d(r_k)!\right) \tag{2.31}$$

The previous equation simplifies to eliminate the exponential term by

$$L = \sum_{k=1}^{N} ln\left(I(r_k)^{d(r_k)}\right) - I(r_k) - ln\left(d(r_k)!\right) \tag{2.32}$$

The term $ln\left(d(r_k)!\right)$ will be a constant as a function of the range parameter after the summation and only serves as a bias to the overall likelihood calculation. Bias terms do not affect the location of maxima or minima points and can be dropped from further expressions. This simplification leaves the log likelihood equation as

$$L = \sum_{k=1}^{N} ln\left(I(r_k)^{d(r_k)}\right) - I(r_k) \tag{2.33}$$

At this point, it is acceptable to substitute in the expression for the model chosen for the intensity of the waveform, $I(r_k)$. For the purpose of this derivation, it will be assumed that Gaussian waveform model shown in Equation (2.3) and described in Section 2.3.2 is chosen as the reference model. Making the substitution for $I(r_k)$ yields the equation

$$L(G, R, \sigma_w) = \sum_{k=1}^{N} ln \left(\left(\frac{G}{\sqrt{2\pi}\sigma_w} e^{\frac{-(r_k - R)^2}{2\sigma_w^2}} \right)^{d(r_k)} \right) - \frac{G}{\sqrt{2\pi}\sigma_w} e^{\frac{-(r_k - R)^2}{2\sigma_w^2}} \tag{2.34}$$

The likelihood function, L, has now been annotated to show that the estimate is a function of the the amplitude of the signal, G, the true range to the target, R, and the standard deviation or pulse width of the Gaussian reference model, σ_w. A separate method based on curve fitting to estimate σ_w will be executed before the maximum likelihood method is performed and is described in Section 3.3. Obtaining an estimate for σ_w will leave two unknowns at this point in the process, R and G.

To estimate G, the derivative of the likelihood function in Equation (2.34) will be found and maximized with respect to G. This step yields an estimation of G as

$$G = \frac{\sum_{k=1}^{N} d(r_k)}{\sum_{k=1}^{N} \frac{1}{\sqrt{2\pi}\sigma_w} e^{\frac{-(r_k - R)^2}{2\sigma_w^2}}} \tag{2.35}$$

which can be placed back into the waveform model, $I(r_k)$. Now, substituting the equation for $I(r_k)$ with the estimate for G into the log likelihood function, $L(G, R)$, yields an equation that is no longer a function of G and R, simply just R.

The closed form solution for R that maximizes $L(R)$ is difficult to obtain, so it is found by iteratively trying different values of range samples until the maximum value of $L(R)$ is found by

$$R_{ML} = R_{gate} \left(\arg\max_{R} L(R) \right) \tag{2.36}$$

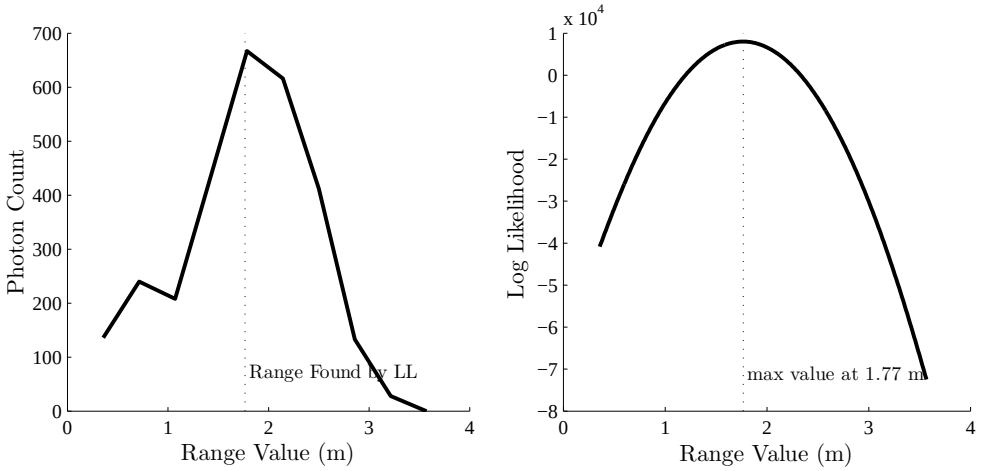

(a) LADAR Return Pulse (b) Log Likelihood Curve

Figure 2.12: a) LADAR signal used in maximum likelihood range estimation algorithm. b) Curve produced by using maximum likelihood algorithm. Maximum value corresponds to range sample returned as estimate by algorithm.

where R_{ML} is the range estimated by the maximum likelihood algorithm. Sub-sample range estimation is achieved by trying a smaller step size between the range sample estimates in question. Figure 2.12 shows an example of the log likelihood plot, with the peak corresponding to the correct range sample.

III. New Techniques in Range Estimation

Chapter III describes a new technique for estimating the range of an object using laser radar, and methods for developing a suitable waveform model for the shape of the laser pulse. An alternative method for reducing gain variation is also presented in Chapter III.

3.1 Alternative Method for Reducing Gain Variation

In addition to the method tested in [7], other ideas have been proposed to reduce the effects of gain variation. In the data collected for this research, an optical filter was placed over the lens of the receiver optics to reduce the amount of light collected by the system. The filter was a 12 nanometer wide bandpass filter with a center of 1.55 micrometers. The filter reduced the total amount of radiation entering the detector and reduced or nearly eliminated the effects of the gain variation. This is shown by the return pulse shapes that appear to be only affected by the shot noise, clock noise, and timing jitter of the system. Figure 3.1 shows an example of some waveforms collected from a target approximately 4.5 meters away with an optical filter in place compared to data from the previous camera system without the use of an optical filter.

3.2 Normalized Matched Filter Algorithm

As described in Section 2.8.2 and shown in Section 5.2 the matched filter range estimation algorithm can produce a bias in waveforms that are not in the center of the range gate. A proposed method to reduce or eliminate this bias is to normalize the energy in each signal using the correlation coefficient.

If the original data waveform is $d(r_k)$, then the normalized signal, $\hat{d}(r_k)$, is defined as

$$\hat{d}(r_k) = \frac{d(r_k) - \bar{d}(r_k)}{\sigma_d} \tag{3.1}$$

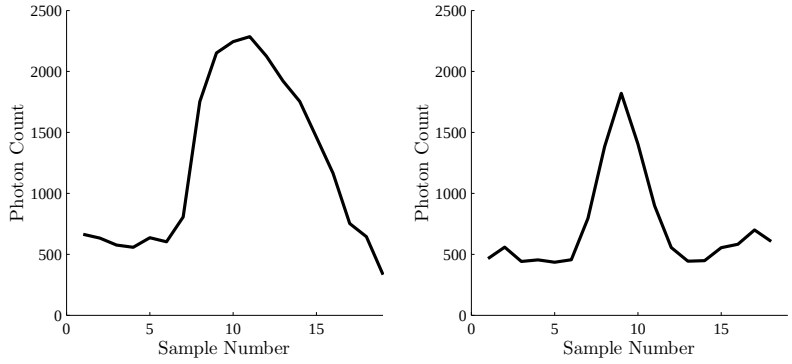

(a) Previous Camera Without Filter

(b) New Camera With Filter

Figure 3.1: a) Waveforms exhibit gain variation which skews return pulse shape when no filter is used. b)LADAR return pulses from camera with use of optical filter to reduce overall intensity and eliminate gain variation; pulses are nearly symmetric

where $\bar{d}(r_k)$ is the mean value of the data and σ_d is the standard deviation of the data waveform defined by

$$\sigma_d = \sqrt{\frac{\sum_{k=1}^{N} \left(d(r_k) - \bar{d}(r_k)\right)^2}{N}} \tag{3.2}$$

where N is the total number of samples in the waveform. The reference waveform, $f(r_k)$, is normalized in the same method and annotated by

$$\hat{f}(r_k) = \frac{f(r_k) - \bar{f}(r_k)}{\sigma_f} \tag{3.3}$$

and

$$\sigma_f = \sqrt{\frac{\sum_{k=1}^{N} \left(f(r_k) - \bar{f}(r_k)\right)^2}{N}} \tag{3.4}$$

where $\hat{f}(r_k)$ is the normalized reference waveform, $\bar{f}(r_k)$ is the mean value of the reference waveform, and σ_f is the standard deviation of the reference waveform data. From here, the range is estimated the same as the time domain matched filter previously described, but now the normalized signals are used in the calculation of the

cross correlation, $\hat{C}_{d,f}(\tau)$, as shown in

$$\hat{C}_{d,f}(\tau) = \sum_{k=1}^{N} [\hat{d}(r_k)\hat{f}(r_k - \tau)] \tag{3.5}$$

The range is estimated by finding the range sample that maximizes Equation (3.5) as described in

$$R_{NCTD} = R_{gate}\left(\arg\max_{\tau} \hat{C}(\tau)\right) \tag{3.6}$$

where R_{NCTD} is the range to the target estimated by the normalized matched filter algorithm performed in the time domain.

The normalized matched filter technique can also be applied by selectively choosing pixels that only show a desired degree of correlation. This selective process is designed with the intent of discarding waveforms that do not match the model and could deliver poor range estimates. The selective normalized matched filter algorithm could potentially help with the sensitivity of the algorithm to deviations from the reference model. This is practical in research purposes when pixel by pixel estimations are performed to analyze the system and algorithms, but in reality all pixels of data may be needed depending on the particular application.

3.3 Reference Waveform Design

Both the matched filter and the maximum likelihood algorithms rely heavily on the assumption that the shape of the return pulse is known. Even after the Gaussian or inverse parabola model is chosen, the algorithms must still know the correct width of the pulse in order to effectively choose the range. This section will present the techniques used to build a reference waveform.

3.3.1 Pulse Width Estimation Techniques. Each of the algorithms presented in this chapter use the same fundamental process to estimate the width of the wave-

form. The pulse width estimation (PWE) technique works by first choosing range of widths to guess at. A reference waveform is created with each guess and centered on the pulse in question. The error is determined by subtracting the two pulses, squaring the error, and finding the mean value. The next value for the pulse width is tried and the process is repeated. This process is also repeated with the reference waveform centered 1-2 samples off center in case the peak of the waveform is shifted due to the effects of shot noise. Each mean square error value is recorded and produces a curve that is used to determine the minimum error. The pulse width guess that produced the least error is chosen as the estimate by the PWE.

Based on the visual observation of the return pulses from the LADAR camera that did not exhibit strong gain variation and skewed pulses, a Gaussian return pulse was used as the basis for the model. It appeared as a better fit to due to the inclusion of tails in the model. The inverse parabolic method did not include this trait. The use of the optical filter produced symmetric waveforms, so the hybrid waveform model was not chosen. An experiment was conducted to determine which of the pulse width estimation techniques would perform the best by using simulated data to compare the results of each technique. The benefit of using simulated data in this case is that the pulse width is known and can be used to determine if there is any bias in the different techniques.

At this point in the process of building the reference waveform, several options are present to choose from. The following techniques were developed and explored during the scope of this research:

3.3.1.1 Averaging Pulses then Estimating. The Averaging Pulses then Estimating (APE) algorithm averages LADAR return pulse waveforms and makes one estimate to use for all the waveforms based on results of the averaged waveform. The APE method is beneficial because only one estimation is made for a large group of pixels which results in a faster algorithm. However, as illustrated by Figure 3.2, averaging different return pulses could result in an averaged pulse that is wider than the

individual returns the estimate is designed for. Target surfaces, range differences, timing jitter, or clock error can all cause pulse widths to vary slightly and shift position. However, if the pulses are properly aligned then the averaging is beneficial because the random noise can be averaged out, resulting in a more accurate estimation.

3.3.1.2 Estimating Widths then Averaging. The Estimating Widths then Averaging (EWA) algorithm estimates the individual pulse width of each waveform in a group of pixels. The reference waveform is built using the mean value of the estimations. EWA is computationally slower than APE, but could be more accurate because it does not depend on the averaged waveform that could be artificially widened due to sources of noise previously described.

3.3.1.3 Estimating Widths No Averaging. The Estimating Widths No Averaging (EWNA) algorithm estimates the individual pulse width of each waveform in a group of pixels the same as the EWA algorithm. The difference between EWA and EWNA is that a separate reference waveform is built for each pixel based off the estimated pulse widths stored in memory. The EWA and EWNA should computationally take the same amount of time, but the EWNA algorithm requires more memory. The results in Section 5.1 will show that for the purposes of this research there is not much benefit to using EWNA versus EWA. In fact, due to error caused by noise in the LADAR return pulses EWNA may actually be less beneficial when creating a reference model because none of the noise is averaged out of the pulse width estimates.

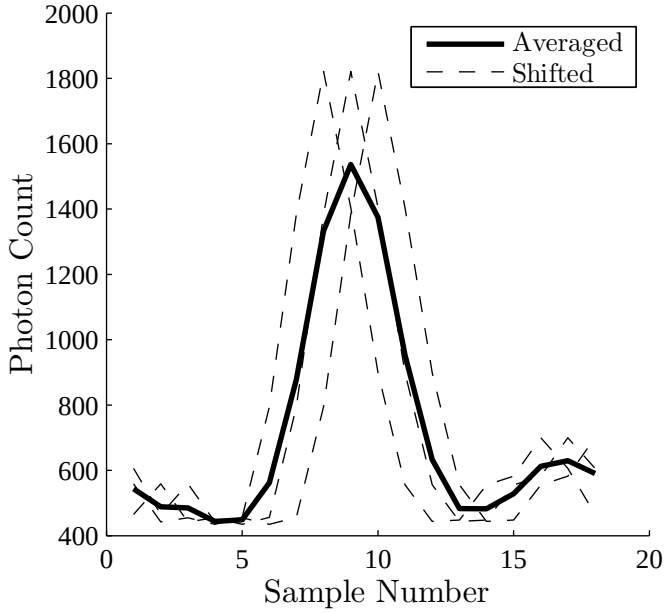

Figure 3.2: LADAR return pulses in different pixels that when averaged form a pulse that is slightly wider than the individual returns.

IV. Methodology

Chapter IV documents the design and setup of different experiments used to test the techniques described in Chapters II and III. Included in this chapter is an additional explanation of the experiment used to analyze the effectiveness of the PWE techniques. The design and setup of the simulated and measured LADAR return pulse collection experiments is also presented in Chapter IV.

4.1 Pulse Width Estimation Experiment Design

To evaluate the PWE technique described in Section 3.3 a simple experiment was designed to estimate pulse widths in simulated data. The data was created in a similar way to that described in Section 4.2. Instead of varying the amplitude or position of the waveforms, a set of Gaussian shaped reference waveforms were created with varying pulse widths ranging from 1 ns to 6 ns in 0.5 ns increments. Figure 4.1 shows an example of several of the pulse widths used in the experiment.

The raw PWE technique was applied to the set of noiseless waveforms and the results were recorded. Next, a 3-D cube of 23 x 23 pixels was made to create 529 waveforms. These values were chosen because it was similar to the amount of pixels available for range estimation in the measured data set. Poisson noise was added to simulate the shot noise created under realistic conditions. This cube of data was used to evaluate the APE, EWA, and EWNA algorithms discussed in Section 3.3. The results were recorded and are presented in Section 5.1.

4.2 Simulated Data Experiment Design

Before the range estimation algorithms were applied to measured LADAR data, a simulation of data was performed. The goal of the simulation was to examine the performance of the range estimation algorithms under hit mode conditions. In order to create an environment for the experiment to be successful, it would be necessary to generate waveforms that were at different positions within the range gate. This section will describe the conditions of that experiment.

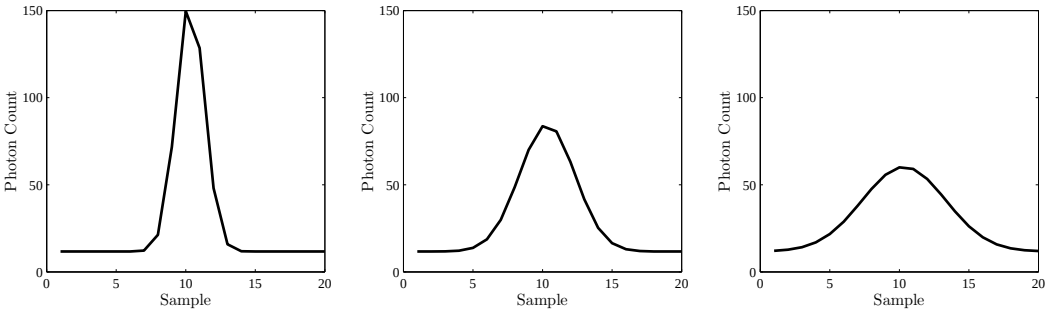

(a) 2 ns pulse width (b) 4 ns pulse width (c) 6 ns pulse width

Figure 4.1: Examples of simulated LADAR waveforms of varying widths used for PWE tests.

In the simulation the target was placed at 100 meters from the receiver. The outgoing pulse was modeled as a Gaussian waveform. The range equation described in Section 2.4 was used to calculate the number of photoelectrons received by the system. Shot noise was added to the waveforms using the Poisson distribution model. The values chosen for the parameters of the range equation are shown in Table 4.1.

Table 4.1: Parameter Values for Simulated Data

Parameter Values			
P_{trans}	1 mJ	Detector Size	1 μm
θ	0.05 radians	Solar Irradiance	1 kW μm/m^2
Focal Length	100 mm	System Bandwidth	500 MHz
D	10 mm	η_D	0.3
λ	1.55 μm	η_{atm}	1
G	20	ρ_t	0.10
R	100 m	q	1.602 $\times 10^{-19} coulombs$
h	6.626 $\times 10^{-34}$ J s		

Data samples were simulated from 80 to 120 meters. Figure 4.2 shows the sample buffered waveform without noise before any hit mode specifications are made to it. Instead of setting a threshold and allowing waveforms to be cropped to achieve the desired positions within the range gate, a 20 sample window was used to shift through the main wave pulse to collect the waveforms. Waveforms could be positioned on the left, center, or right side of the range gate. In addition, waveforms at the edges of the range gate were allowed to shift outside of the range gate in order to clip the amplitude

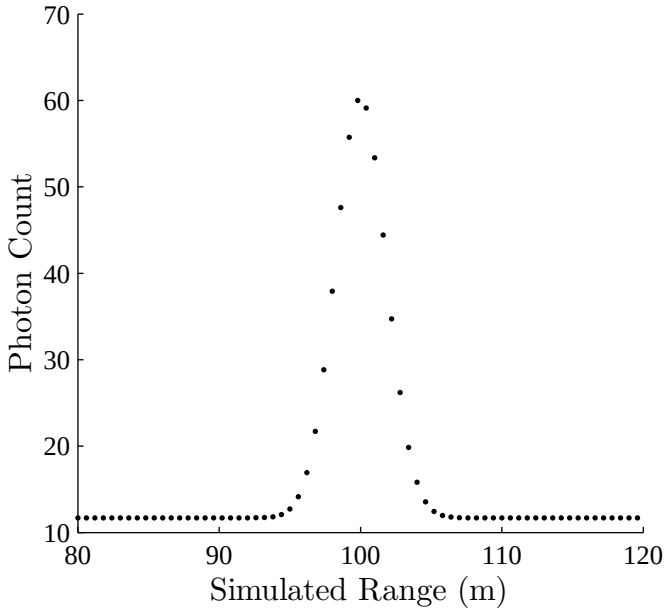

Figure 4.2: Simulated noiseless data buffered through LADAR sytem

before the true peak of the original waveform was reached. A total of 20 waveforms were created and used as the basis for the noisy waveform range estimations. Figure 4.3 shows an example of several of the waveforms created for the simulation.

After creating the 20 waveforms, the next step was to add simulated shot noise to each waveform. After the random noise was added, the range to the target was estimated using each of the range estimation techniques. The process of adding noise and estimating the range was repeated 1000 times for each waveform.

The sampling rate of the simulated system allows for the collection of a data point at about every 60 cm. As shown in Figure 4.4 the true peak of the waveform should be at 100 m, but due to the sampling rate the closest samples to the peak are contained at 99.8 and 100.4 meters. Without some form of sub-sample interpolation, these are the closest values a range estimation technique without interpolation will find.

In addition to testing the various range estimation algorithms, the PWE algorithms (APE, EWA, and EWNA) were also tested in conjunction with the estimation

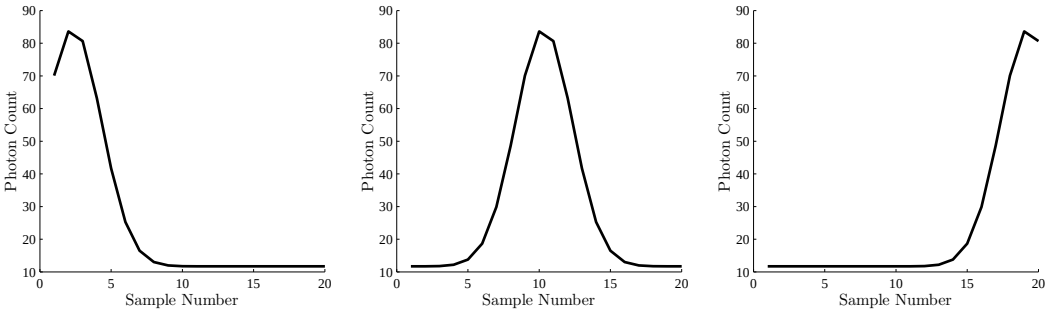

(a) Left Side of Range Gate (b) Center of Range Gate (c) Right Side of Range Gate

Figure 4.3: Examples of waveforms created in various positions in the range gate used in the simulated experiment.

techniques that depend on the standard deviation. The true pulse width was known so algorithms were also tested using the known value for the pulse width. Several different interpolation strategies were also tested with the peak estimator in simulated data to determine if better results could be obtained in the presence of the simulated shot noise. The results of the simulated experiment are presented in Section 5.2.

4.3 Measured Data Experiment Design

Measured data was collected from the ASC 3-D flash LADAR camera in November 2008 at Wright-Patterson AFB using equipment provided by the Air Force Research Laboratory (AFRL) Sensors Directorate Electro-Optics Division (RYJ). This section will describe the conditions and the design of that experiment.

The camera and laser were attached to a platform approximately 4.25 - 4.88 meters from two target boards. The target boards were were made of a styrofoam poster board material about 0.635 cm thick and were not coated with any additional materials to affect the reflectivity of the targets. The target boards were placed between 1.22 - 1.83 meters apart from one another and kept perpendicular to the line of sight of the LADAR system. The two target boards were spaced horizontally in a fashion that would allow the edge of the near board to overlap with the far board and allow both to be seen in the FOV of the LADAR camera. Figure 4.5 is used to

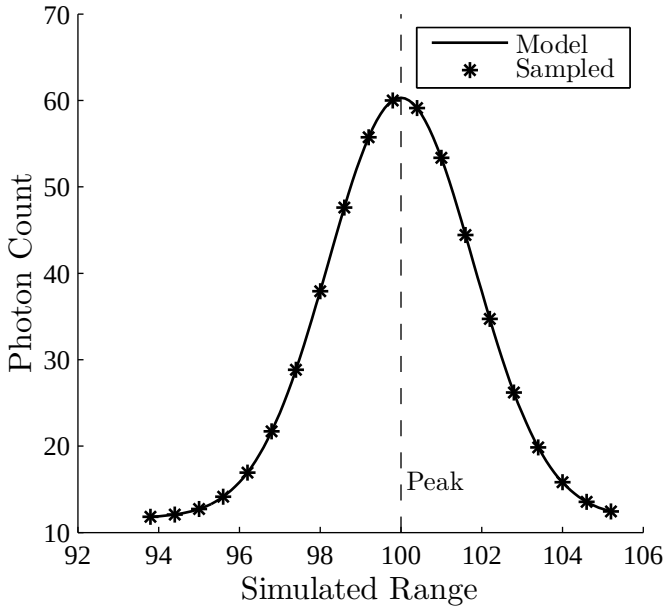

Figure 4.4: Comparison of sampled waveform to original model where peak value is not sampled and illustrates need for sub-sample considerations in range estimation algorithms.

illustrate the set up of the measured data collection. The design of the experiment allowed a range difference between the two boards to be determined from the range estimation algorithms instead of an absolute range. The method of examining range differences versus absolute range was chosen because using a range difference measurement eliminates the timing jitter noise and allows measurements from different clock cycles to be compared to one another. For example, if the model of the data at one range instance, $d_n(r)$, with the timing jitter noise added to the waveform is

$$d_n(r) = d(r) + n_{tj} \tag{4.1}$$

where $d(r)$ is timing jitter noise free data, and n_{tj} is the timing jitter noise, then subtracting two measurements, $d_{n1}(r)$ and $d_{n2}(r)$, from the same cube of data where

the timing jitter is the same would yield

$$\begin{aligned} d_{n1}(r) &= d_1(r) + n_{tj} \\ d_{n2}(r) &= d_2(r) + n_{tj} \end{aligned}$$

$$\begin{aligned} d_{n1}(r) - d_{n2}(r) &= d_1(r) + n_{tj} - (d_2(r) + n_{tj}) \\ \Delta D(r) &= d_1(r) + n_{tj} - d_2(r) - n_{tj} \\ \Delta D(r) &= d_1(r) - d_2(r) \end{aligned} \tag{4.2}$$

where $\Delta D(r)$ is a range difference measurement between two pixels.

100 pulses were fired from the camera in order to collect enough data to attempt to average out the noise over the multiple frames of data. Each pulse creates a 3-dimensional cube of data made with the pixel location corresponding to the y- and x- axes and the photoelectron intensities of the waveforms registering along the range axis.

The target boards were placed at different distances to attempt to create waveforms that would be captured either on the left side, center, or right side of the range gate to recreate the conditions of experiment performed with simulated data.

Table 4.2 lists the data files collected and the difference in range between the two boards that would serve as a truth measurement when testing for bias in the range estimation algorithms. The files were saved in a .SEQ format, which could be

Table 4.2: File names for measured data collection experiment and range difference truth values.

File Name	Range Difference (m)
Sular9ft1.SEQ	1.1938
Sular9ft2.SEQ	1.4732
Sular19ft1.SEQ	1.3462
Sular19ft2.SEQ	1.8542

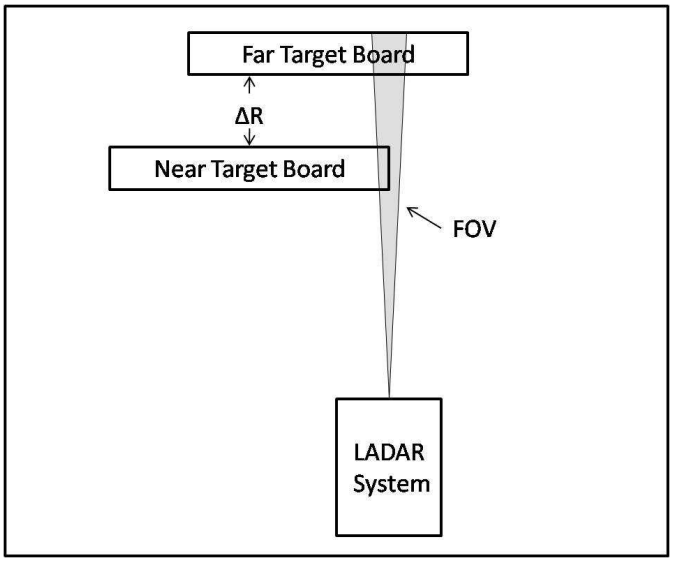

Figure 4.5: Illustration of measured data collection set up.

read into Matlab®. Section 4.3.1 will describe the methods used to process the data and prepare it for the range estimation algorithms.

4.3.1 Processing of .SEQ files. The data collected from the camera was exported to an attached laptop and stored for further use. Data contained in the .SEQ files was read into Matlab® via functions provided by AFRL/RYJ personnel. The data extracted from a .SEQ file was organized into data structures for easy navigation through the information. Each data cube corresponds to a pulse fired from the laser and is stored as a frame of data. The samples stored in each cube of waveforms are initially placed out of order based on the location of a marker slice as shown in Figure 4.6. The sample immediately following the marker slice corresponds to the location of the first sample of data. Information contained in the marker slice is not useful to range estimations and is removed from the sample set thus reducing the overall number of usable samples per waveform to 19.

After sorting the cubes of data and removing the marker slice, the next step was to process each cube and apply the range estimation algorithms. In order to build a reference waveform for the matched filters and maximum likelihood algorithms, the

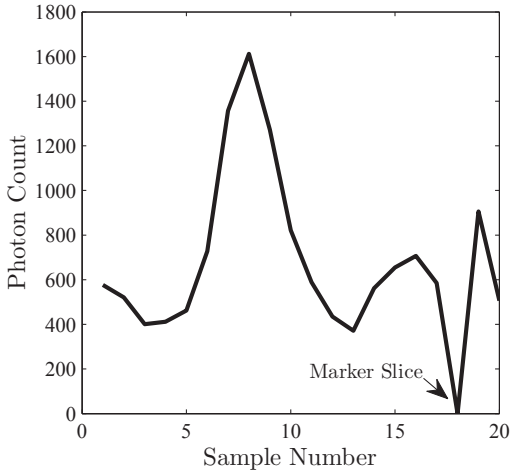

Figure 4.6: Example of a LADAR pulse that has not yet been sorted. Minimum, zeroed out, value is good indication of location of marker slice in data.

pulse widths of the waveforms were estimated using the methods described in Section 3.3. In the first two sets of data collected, the noise levels were too high in the first 10 samples and overpowered the rest of the waveform. These 10 noisy samples were removed from the data set. In the second two sets of data, where the closest target board was moved further away from the camera, the first sample was too noisy and was removed from the data set. Figure 4.7 shows a waveform that has been sorted based on the marker slice and contains overly noisy samples. As the target boards were moved further away, waveforms without the initial noisy samples were obtained, leading one to believe there is a minimum range at which the ASC 3-D flash LADAR system can operate.

The first two files were taken with the camera approximately 4.25 meters from the first board. Based on the fact that the first 10 samples were always dominated by background noise, it appears that the camera has a minimum range of approximately 3.5 meters. This was not further tested during the experiments and is just a side observation that could prove useful in future tests. When the target boards were moved further away, the noisy samples were reduced to 1 sample that had to be removed from the waveforms. Figure 4.8 shows a set of intensity images revealing the

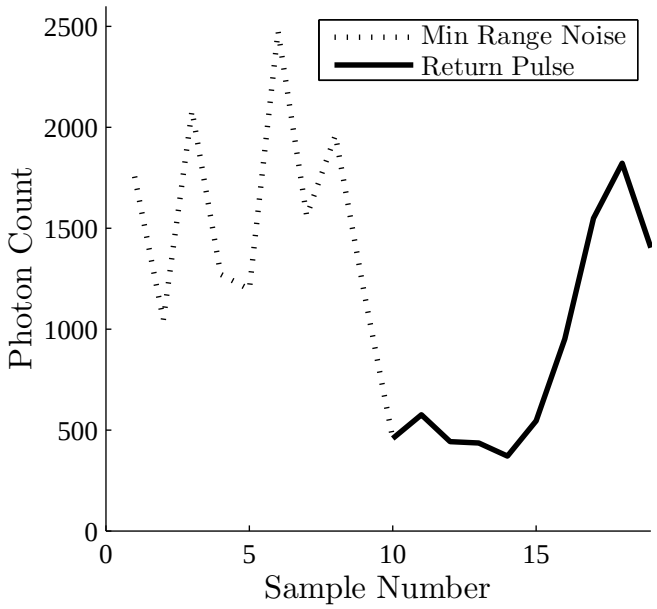

Figure 4.7: Example of LADAR return pulse that after being sorted based on marker slice, the first samples exhibit a high degree of background noise. Possible evidence of a minimum range for detection by ASC 3-D flash LADAR system.

two target boards. The near board is seen in sample slice 3, and the far board is seen in sample slice 8. The information shown in Figures 4.8 - 4.10 is taken from data set Sular19ft2.SEQ and provides a fair representation of the other data sets. Figure 4.9 shows a set of waveforms from row 80 to give an example of the variation among waveforms used in range estimation. Figure 4.10 shows how the difference in range between the two target boards can be roughly estimated by looking at the difference in samples between the waveforms.

4.3.2 Application of Range Estimation Algorithms. In total, 16 different variations of the range estimation algorithms were applied to the measured data set. The peak estimator was applied with no interpolation, linear interpolation, cubic spline interpolation, and shape preserving spline interpolation of the waveform. The matched filter was implemented in the time and frequency domain using the three different PWE techniques. The three PWE techniques were also applied to both the maximum likelihood estimator and normalized matched filter algorithm. The 16

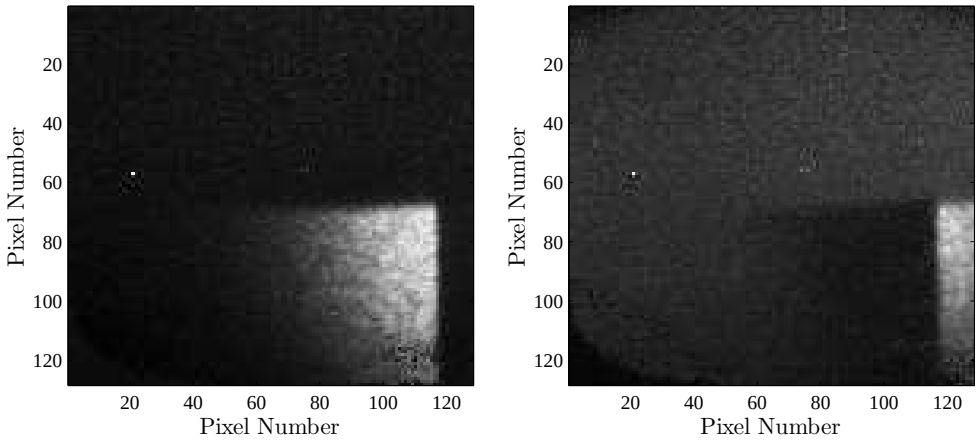

(a) Near Board Intensity Image (b) Far Board Intensity Image

Figure 4.8: Intensity images from set of data when target boards were 1.85 meters apart. Near board image in (a) is from cube slice 3 and far board image in (b) is from cube slice 8.

combinations of range estimation were applied to each of the 4 sets of data using an area of approximately 121 pixels and then 500 pixels. The larger region of pixels was used to determine if branching out to the noisier pixels at the edge of the camera's field of view would affect the range estimation results. The results of the experiments are presented in Section 5.3.

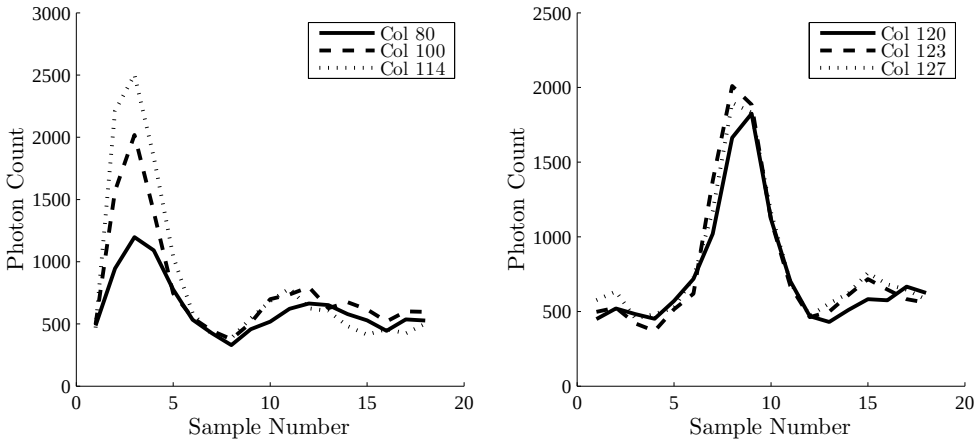

(a) Near Board Waveforms (b) Far Board Waveforms

Figure 4.9: Waveforms taken from pixel row 80 looking at data from various columns in both the near and far board returns.

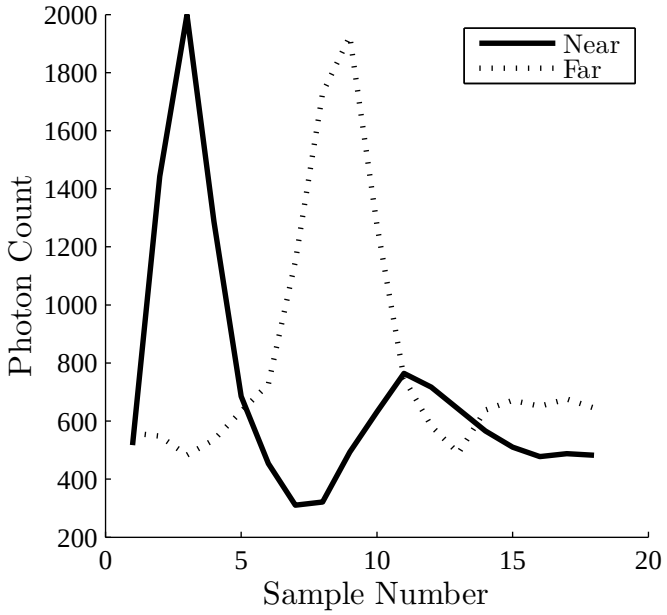

Figure 4.10: Comparison of waveforms from near board versus far board. Actual distance between target is 1.85 meters or about 5.18 samples

4.4 Methods for Analyzing Results

This section describes the processes and metrics used to determine the effectiveness of the range estimation techniques.

4.4.1 Simulated Data. In the simulated data, the true range to the target was 100 meters. To test for bias in range measurements, the Root Mean Square Error (RMSE) in each of the 20 waveform positions for an estimation technique was computed using

$$RMSE = \sqrt{\frac{\sum_{n=1}^{N}(R - \hat{R}_n)^2}{N}} \tag{4.3}$$

where R is the true location of the target, $\hat{R}_n$ is the estimated range found by the algorithm in noisy waveform n, and N is the total number of measurements (1000). The RMSE is in units of meters.

To test for the stability of the estimation techniques, the standard deviation in the measurements was also found. Standard deviation was calculated using

$$\sigma_{error} = \sqrt{\frac{\sum_{n=1}^{N}(\hat{R}_n - \bar{r})^2}{N}} \tag{4.4}$$

where $\bar{r}$ is the mean value of the estimates. The σ_{error} is in units of meters.

In total, 20 RMSE and σ_{error} calculations were found for each range estimation algorithm. This would allow the error to be plotted as a function of waveform position within the range gate. In addition to these two calculations of error as a function of waveform position, the average RMSE and standard deviation was also calculated for waveforms in the center and edge of the range gate.

The total error was found by treating the RMSE and σ_{error} as two independent random variables whose sum could be found by

$$Error_{tot} = \sqrt{RMSE^2 + \sigma_{error}^2} \tag{4.5}$$

where $Error_{tot}$ is in units of meters.

4.4.2 Measured Data. In the data collected from the ASC 3-D flash LADAR camera, a similar method for finding the RMSE and variance is used to analyze the results. The RMSE and σ_{error} were calculated for each range estimation technique using Equations (4.3) and (4.4). In the measured data sets, range differences between the two target boards were used as the basis for the range measurement. For each of the 100 cubes of data, the range difference was found by subtracting the distance to each pixel in the far board from the distance to each pixel in the near board. The mean value of the range difference was then used as the range difference value for a particular cube. The mean value could be plotted as a function of the cube number or laser pulse time. This analysis, presented in Chapter V would show the measurements as a function of time and allow the user to see if there was any indication of a trend in the clock based on the results. Among these average values, the RMSE error was found and the standard deviation was also calculated. The total error was also calculated using Equation (4.5).

Results were also analyzed by examining differences in the results based on the number of pixels used in the calculated the estimation. Tests were run with either approximately 121 or 500 pixels. In addition the results were also analyzed based on which PWE algorithm was used as described in Section 3.3.

V. Results

Chapter V contains the results of the simulated and measured data results.

5.1 Pulse Width Estimation Experiment Results

5.1.1 PWE Results with Noiseless Data. To test for bias in the PWE technique, the PWE algorithm was first applied to a set of waveforms that had no noise added. With the exception of the narrowest pulse widths, the estimator performed perfectly. Table 5.1 shows the true and estimated values of the PWE algorithm under noiseless scenario. The average error in the experiment was 0.023 ns. The error in the narrowest pulse widths is due to undersampling of the signal which misled the algorithm. Based on the results obtained in this experiment it is feasible to assume the technique is unbiased without noise present. The experiment was continued by testing the PWE technique on waveforms with noise added.

Table 5.1: Results of noiseless PWE experiment show the lack of bias in the estimator.

Actual Pulse Width (ns)	Est. Pulse Width (ns)	Error (ns)
1.0	1.2	0.2
1.5	1.6	0.1
2.0	2.0	0
2.5	2.5	0
3.0	3.0	0
3.5	3.5	0
4.0	4.0	0
4.5	4.5	0
5.0	5.0	0
5.5	5.5	0
6.0	6.0	0

5.1.2 PWE Results with Noisy Data. The next step was to conduct the same experiment but with Poisson distributed noise added to the waveforms. 529 noisy waveforms were used to simulate a 23 x 23 array of pixels. The PWE estimation technique was applied via the APE and EWA methods to determine if there were any conclusions that could be drawn regarding the performance of the PWE algorithm

in a noisy environment. In the APE algorithm experiment, the waveforms were first averaged and then used to find the pulse width. Table 5.2 shows the results of the PWE experiment using the APE algorithm. The results were the same as when the PWE technique was applied to noiseless waveforms. This shows that the Poisson distributed noise can be mitigated from waveforms by averaging them. However, if the waveforms have shifted positions due to range differences or timing jitter then averaging could produce a waveform that is wider than the original pulse as shown in Figure 3.2. To test the EWA method, the individual pulse width was calculated for

Table 5.2: Results of PWE experiment when using APE algorithm.

Actual Pulse Width (ns)	Est. Pulse Width (ns)	Error (ns)
1.0	1.2	0.2
1.5	1.6	0.1
2.0	2.0	0
2.5	2.5	0
3.0	3.0	0
3.5	3.5	0
4.0	4.0	0
4.5	4.5	0
5.0	5.0	0
5.5	5.5	0
6.0	6.0	0

each simulated pixel's waveform. The mean value of the pulse width estimate over the 529 pixels was recorded as the EWA estimate. Table 5.3 lists the results of the EWA experiment. The average error was 0.1545 ns which is an order of magnitude greater than the APE method. There is also a noticeable increase in the standard deviation of the pulse width estimates as the pulse width increases. In the measured data, however, it may prove more effective to to implement the EWA or EWNA method when determining the range due to the slight shifts in waveforms that could occur.

5.2 Range Estimation Simulated Experiment Results

The simulated experiment described in Chapter IV was performed with both noiseless and noisy waveforms. The results are presented in the following sections.

Table 5.3: EWA results

Actual Pulse Width (ns)	Avg. Est. Pulse Width (ns)	Error (ns)	σ (ns)
1.0	1.280	0.280	0.0535
1.5	1.641	0.141	0.0804
2.0	2.107	0.107	0.1295
2.5	2.633	0.133	0.1990
3.0	3.124	0.124	0.2635
3.5	3.673	0.173	0.3314
4.0	4.213	0.213	0.4071
4.5	4.686	0.186	0.4469
5.0	5.168	0.168	0.5201
5.5	5.635	0.135	0.5725
6.0	6.040	0.040	0.6428

5.2.1 Results of Simulation Without Noise. To test for any natural bias in the range estimation algorithms, the simulation was conducted first on noiseless waveforms. Different interpolation methods were applied to the peak estimator algorithm. The pulse width dependent waveforms used the EWNA pulse width estimation technique as well as the known pulse width value. The other PWE methods were not applied because they would be irrelevant without noise added. Because noise was not added to the signal, only one trial was performed for each waveform. Only the RMSE was calculated, because the standard deviation is undefined for one measurement.

Table 5.4 lists the average RMSE of the range estimation algorithms at both the center 10 samples and the 10 samples on the left and right side of the range gate. The only unbiased estimators are the peak estimator using the spline method and the normalized matched filter. The matched filter in the time domain and maximum likelihood show a low average RMSE (1 mm and 3 mm respectively) in the center of the range gate. In contrast, for waveforms shifted off center the matched filter in the time domain produced an average RMSE of 0.310 m while the maximum likelihood algorithm produced a slightly higher average RMSE of 0.315 m. The frequency domain implementation of the matched filter has an average RMSE of 0.225 m in the center and 0.297 at the edges of the range gate. As seen in Figure 5.1 the frequency domain

implementation of the matched filter is not as sensitive in the bias caused by off center waveforms, but still has an overall bias in even the centered waveforms.

Table 5.4: Results of simulation of range estimation when no noise is added to waveforms.

	RMSE Center (m)	RMSE Edge (m)
Peak Estimator		
No Interpolation	0.200	0.200
Linear Interpolation	0.200	0.200
Spline Interpolation	0.000	0.020
Pchip Interpolation	0.200	0.200
Matched Filter Time Domain		
Known Width	0.001	0.310
EWNA	0.001	0.310
Matched Filter Freq Domain		
Known Width	0.225	0.297
EWNA	0.225	0.297
Maximum Likelihood		
Known Width	0.003	0.315
EWNA	0.003	0.315
Normalized Matched Filter		
Known Width	0.000	0.000
EWNA	0.000	0.000

Figure 5.2 shows a comparison of the average range found by the different interpolation methods of the peak estimator. Because no noise was added, the only error in the results is produced from interpolation or sampling error. Interpolation of the waveform was implemented using the built in interpolation packages in Matlab®. The peak estimator has approximately the same average RMSE for both the centered and non centered waveforms. The only difference in error occurs when a waveform's peak was located outside of the range gate. The peak estimator is able to perform accurately in a noiseless environment using the spline estimator, but cannot account for waveforms that have a cropped peak.

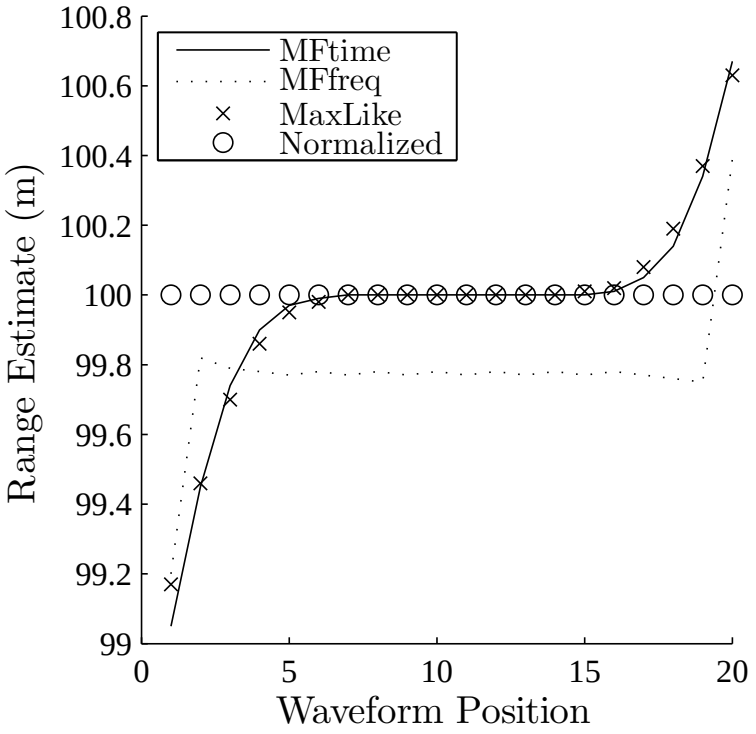

Figure 5.1: Average range determined by matched filters (time domain, frequency domain, and normalized) and maximum likelihood estimators. Results are from noiseless simulation where true location of target was at 100 meters. A 1 value for waveform position indicates a waveform on the far right side of range gate. A 20 value for waveform position indicates a waveform on the far left side of the range gate.

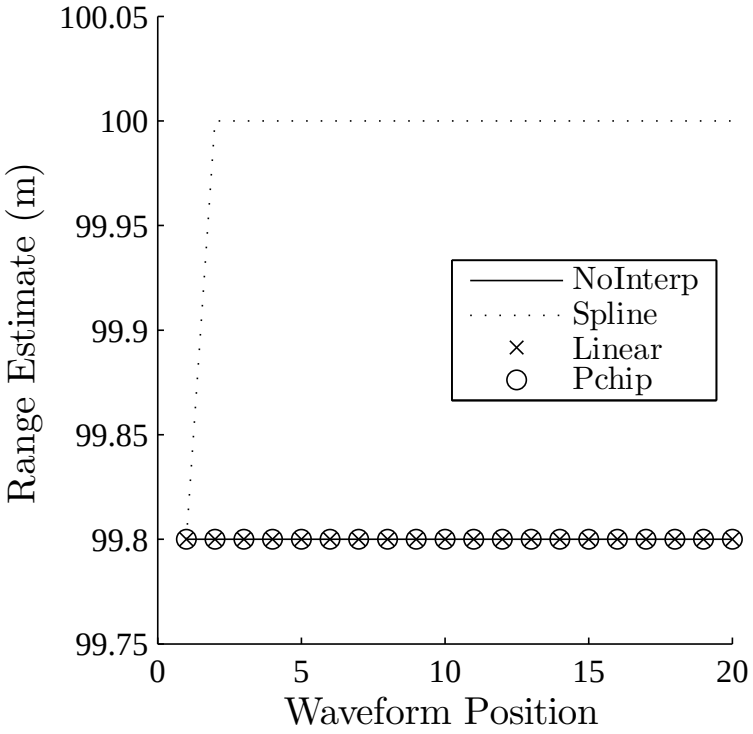

Figure 5.2: Average range determined by peak estimator as waveforms change position within range gate in noiseless simulation. True location of target was 100 meters. A 1 value for waveform position indicates a waveform on the far right side of range gate. A 20 value for waveform position indicates a waveform on the far left side of the range gate.

5.2.2 Results of Simulation With Noise. After the noiseless simulation, range estimation algorithms were tested against 1000 noisy versions of the 20 different waveforms as they shifted position through the range gate. The results are compared based on RMSE and standard deviation of the measurements found. An average RMSE and standard deviation value of the 20 waveform positions is also calculated to compare the overall performance of the algorithms. In addition to testing the range estimation algorithms, the three PWE estimate techniques (APE, EWA, and EWNA) were also examined. Table 5.5 lists the average RMSE and standard deviation values of the range estimation techniques for the simulation with noise.

5.2.2.1 Peak Estimator. Figure 5.3 shows the average range found by the peak estimator algorithm as the waveforms shift position within the range gate. The RMSE with respect to waveform position is illustrated in Figure 5.4. Over the center 10 waveforms, the peak estimator had the largest average RMSE of about 0.345 m. This is approximately the same as the average RMSE at the edges of the range gate, as shown in Table 5.5. The peak estimator appears to be unaffected by waveform position as long as the peak is contained in the range gate, but it is grossly affected by the noise and level of interpolation. As shown in Figures 5.3 - 5.5 the raw uninterpolated waveform does not achieve the results of the interpolated waveforms. The cubic spline method of interpolation is the most effective at reducing error caused by interpolation, even in the presence of the Poisson noise.

The standard deviation of the peak estimator does not change much as it shifts within the range gate and is the highest value of all methods in the center of the range gate. Figure 5.5 shows the standard deviation of the peak estimators with respect to waveform position. The drop in standard deviation at the edges is due to the cropped waveforms that may have not contained the true peak. The smaller amplitudes of the cropped waveforms produces less noise added from the Poisson distribution which may have contributed to less variance among the measurements as the peak was less likely to shift position.

Table 5.5: Results of simulation of range estimation when Poisson noise is added to waveforms. All values have units of meters.

	RMSE Center	RMSE Edge	Std Dev Center	Std Dev Edge
Peak Estimator				
No Interpolation	0.3638	0.3611	0.3635	0.3458
Linear Interpolation	0.3631	0.3603	0.3628	0.3451
Spline Interpolation	0.3296	0.3257	0.3295	0.3057
Pchip Interpolation	0.3638	0.3611	0.3635	0.3458
Matched Filter Time Domain				
Known Width	0.0883	0.3355	0.0883	0.0730
APE	0.0883	0.3300	0.0883	0.0728
EWA	0.0868	0.3456	0.0867	0.0715
EWNA	0.0874	0.3514	0.0874	0.0928
Matched Filter Freq Domain				
Known Width	0.3051	0.3733	0.3036	0.2881
APE	0.3051	0.3633	0.3036	0.2971
EWA	0.3005	0.3355	0.2984	0.2423
EWNA	0.2993	0.3785	0.2970	0.3162
Maximum Likelihood				
Known Width	0.1732	0.4430	0.1732	0.3074
APE	0.1732	0.4450	0.1732	0.3065
EWA	0.1732	0.4430	0.1732	0.3109
EWNA	0.1732	0.4419	0.1732	0.3139
Normalized Matched Filter				
Known Width	0.0886	0.1241	0.0886	0.1239
APE	0.0886	0.1291	0.0886	0.1206
EWA	0.0872	0.1381	0.0871	0.1249
EWNA	0.0878	0.1798	0.0878	0.1646

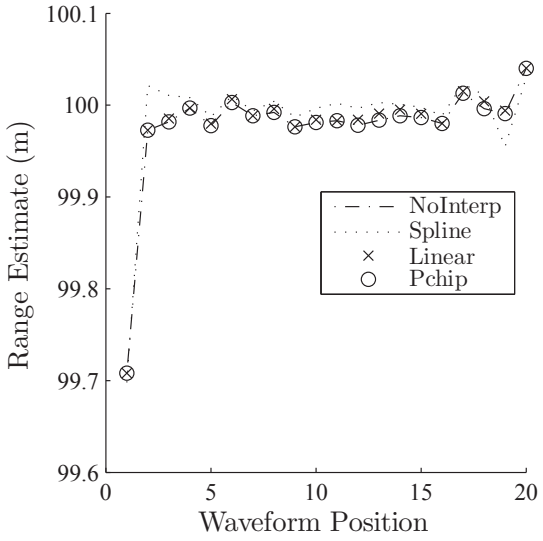

Figure 5.3: Average range determined by peak estimator as waveforms change position within range gate. True target location was 100 meters. A 1 value for waveform position indicates a waveform on the far right side of range gate. A 20 value for waveform position indicates a waveform on the far left side of the range gate.

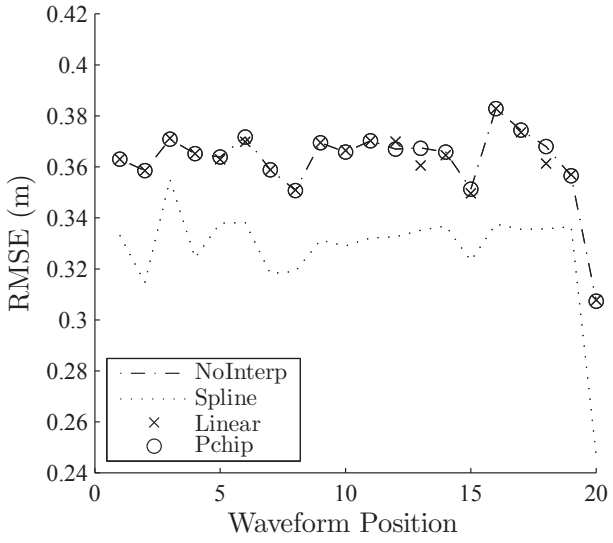

Figure 5.4: RMSE of peak estimator algorithm as waveforms change position within range gate. A 1 value for waveform position indicates a waveform on the far right side of range gate. A 20 value for waveform position indicates a waveform on the far left side of the range gate.

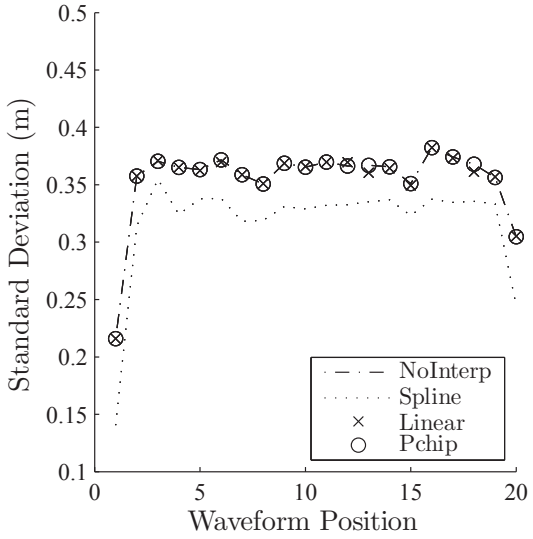

Figure 5.5: Standard deviation of peak estimator results as waveforms change position within range gate. A 1 value for waveform position indicates a waveform on the far right side of range gate. A 20 value for waveform position indicates a waveform on the far left side of the range gate.

5.2.2.2 Matched Filter. Based on the results of the simulation without noise, both the matched filters in the time and the frequency domains were expected to show a bias in the range measurements at the edges of the range gate. As shown by Figures 5.6 the matched filter techniques underestimate the range when the waveform is shifted left of center and overestimate the range when the waveform is shifted to the right of center. This is also seen in the RMSE plots shown in Figure 5.7 as the error drops dramatically in the center of the range gate and rises with the first and last 3 waveforms. The frequency domain implementation of the matched filter does a better job of adapting to the shifting waveforms than the time domain counterpart as indicated by the lower RMSE at the edges of the range gate. However, the matched filter in the time domain has a lower overall bias due to its stronger performance with the waveforms that are centered in the range gate. In the center of the range gate the matched filter time domain implementation had the lowest RMSE of the different range estimation techniques tried with an average RMSE of under approximately 0.088 m and an average standard deviation over the same interval of about 0.073 m. The frequency domain implementation produced an error of approximately 0.373 m over the center samples, which is not any better than the peak estimator.

The three different PWE algorithms were tested alongside a comparison to using the known standard deviation with both matched filter techniques. There was not a dramatic difference in the results, which could be due to the fact that timing jitter noise was not simulated to cause waveforms to shift. The matched filter in the frequency domain does appear to be slightly more sensitive to the changes in the PWE technique, while the time domain version does not appear to be too sensitive based on the technique used. Table 5.5 lists the results broken down by PWE technique for comparison.

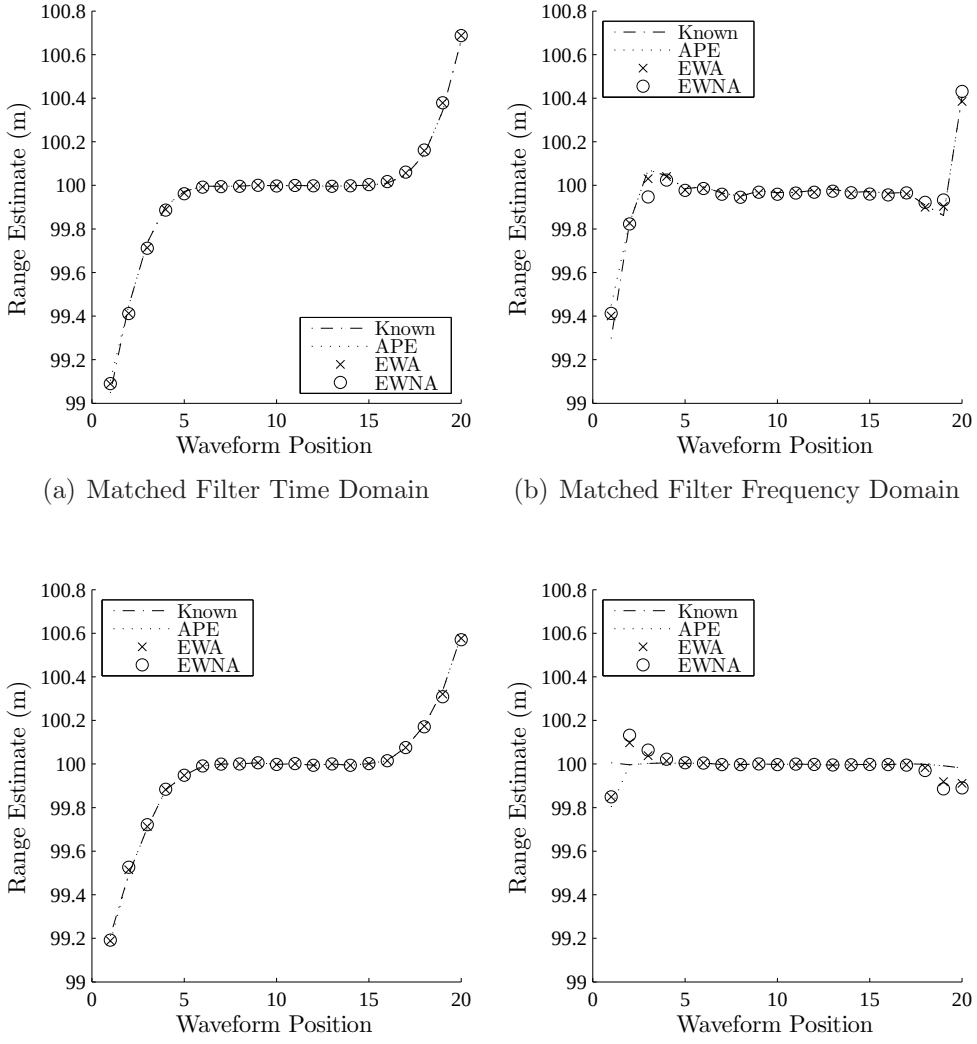

(a) Matched Filter Time Domain

(b) Matched Filter Frequency Domain

(c) Maximum Likelihood

(d) Normalized Matched Filter

Figure 5.6: Average range found by matched filter and maximum likelihood estimators in simulation with noise added. True target location is 100 meters. A 1 value for waveform position indicates a waveform on the far right side of range gate. A 20 value for waveform position indicates a waveform on the far left side of the range gate.

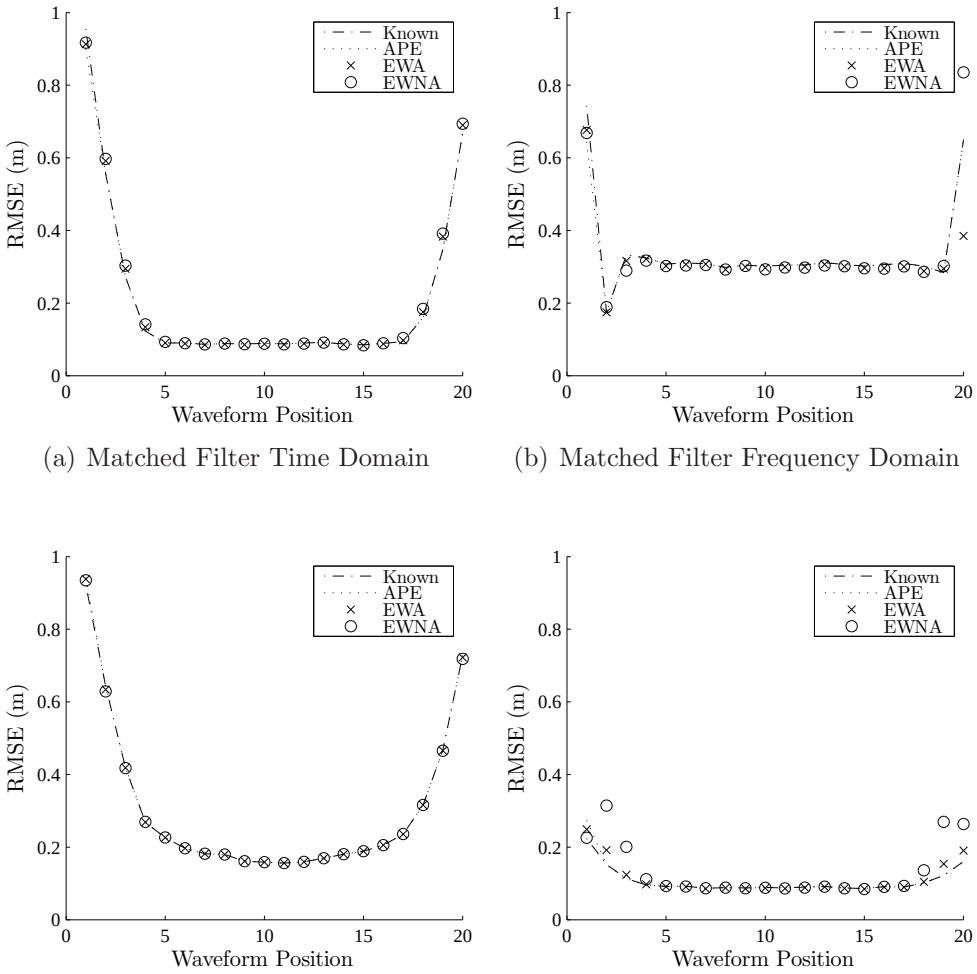

(a) Matched Filter Time Domain

(b) Matched Filter Frequency Domain

(c) Maximum Likelihood

(d) Normalized Matched Filter

Figure 5.7: RMSE found by matched filter and maximum likelihood estimators in simulation with noise added. A 1 value for waveform position indicates a waveform on the far right side of range gate. A 20 value for waveform position indicates a waveform on the far left side of the range gate.

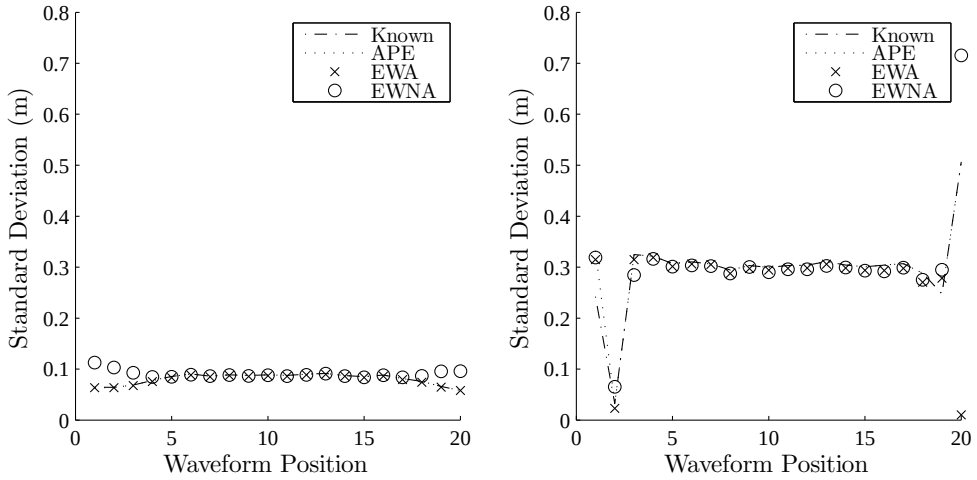

(a) Matched Filter Time Domain

(b) Matched Filter Frequency Domain

(c) Maximum Likelihood

(d) Normalized Matched Filter

Figure 5.8: Standard deviation of range measurements found by matched filter and maximum likelihood estimators in simulation with noise added. A 1 value for waveform position indicates a waveform on the far right side of range gate. A 20 value for waveform position indicates a waveform on the far left side of the range gate.

5.2.2.3 Maximum Likelihood. The maximum likelihood estimator performed similarly to the matched filter in the time domain with respect to the RMSE. Its average error was worse with an average RMSE of about 0.173 cm over the center 10 waveforms. It displayed the strongest reaction to off centered waveforms, with a an average RMSE of 0.443 m over the 10 off center waveforms. The ML estimator, while dependent upon waveform models, was the least sensitive to changes in PWE technique. It appears that while the underlying model of a Gaussian pulse with Poisson noise distribution for the waveform is important in determining an accurate range estimate, the algorithm is not very sensitive to the actual estimates used for the pulse width. The degree to which a pulse width estimate can be incorrect and still yield an accurate result was not explored any further.

5.2.2.4 Normalized Matched Filter. The normalized matched filter was chosen for implementation to remove the bias in range measurements caused by off center waveforms. Figures 5.6 and 5.7 show that the bias that occurs due to waveform position and unbalanced energy levels is successfully removed from the estimations when using the normalization technique before correlation. The normalized matched filter, however, does not improve the standard deviation of the measurements in the center of the range gate as seen in 5.8. This is likely due to the mean value of the results increasing so any deviation from the truth estimate appears as a larger error in the standard deviation.

When using the known value for the pulse width, the normalized matched filter produces excellent results that reduce the bias from measurements caused by waveform position. In comparison to the time domain matched filter, the normalized matched filter offered an improvement in average RMSE of 0.211 m in the edge of the range gate when using the known pulse width. However, when using the alternate methods of EWA or EWNA, the bias is increased up to 0.18 m. It appears from the results of the simulation with noise added that the normalized matched filter is very sensitive to errors in the pulse width estimate and does not perform much better than the matched

filter in the time domain when the pulse width estimate is inaccurate. The APE algorithm performed satisfactorily because it averaged out the noise before estimating the pulse width.

5.2.3 Overall Performance of Algorithms in Simulated Data. It can be seen from the results in the simulation that the strongest performer in reducing the bias produced from random noise and shifted waveforms is the normalized matched filter. The maximum likelihood and time domain matched filter estimators also deliver favorable results, while the peak estimator and matched filter in the frequency domain produce the largest error.

5.3 Measured Data Results

The first sets of data were processed using an 11 x 11 region of pixels that showed the brightest intensity. The smaller region of high intensity pixels were chosen because in theory the stronger signals would produce better range estimates as the Signal-to-Noise Ratio (SNR) was increased. Four data sets were collected, and the average range differences were found for each scenario. Similar to the simulated data, the PWE algorithms were tested alongside the range estimation techniques. Data was also processed using an area that contained approximately 500 pixels to see what would happen when a wider range of signal strengths were used to process the range estimation algorithms. The results of the 4 data sets were averaged, and the average RMSE, average standard deviation, and average total error are presented in Tables 5.6 and 5.7. The results of the individual data sets are contained in Appendix A.

Table 5.6: Results of measured data experiment using 121 pixels to find average range difference.

	Avg RMSE (m)	Avg Std Dev (m)	Avg Total Error (m)
Peak Estimator			
No Interpolation	0.2053	0.0675	0.2225
Linear Interpolation	0.1908	0.0509	0.2029
Spline Interpolation	0.1608	0.0467	0.1719
Pchip Interpolation	0.2044	0.0601	0.2189
Matched Filter Time Domain			
APE	0.1011	0.0568	0.1189
EWA	0.1065	0.0640	0.1277
EWNA	0.1025	0.0590	0.1214
Matched Filter Freq Domain			
APE	0.2144	0.0671	0.2286
EWA	0.2253	0.0868	0.2487
EWNA	0.2228	0.0848	0.2447
Maximum Likelihood			
APE	0.3966	0.0492	0.4016
EWA	0.3965	0.0491	0.4016
EWNA	0.3966	0.0492	0.4017
Normalized Matched Filter			
APE	0.1330	0.0414	0.1432
EWA	0.1433	0.0591	0.1613
EWNA	0.1398	0.0528	0.1549

Table 5.7: Results of measured data experiment using approximately 500 pixels to find average range difference.

	Avg RMSE (m)	Avg Std Dev (m)	Avg Total Error (m)
Peak Estimator			
No Interpolation	0.2195	0.0540	0.2263
Linear Interpolation	0.2017	0.0411	0.2061
Spline Interpolation	0.1755	0.0333	0.1791
Pchip Interpolation	0.2138	0.0421	0.2183
Matched Filter Time Domain			
APE	0.0932	0.0648	0.1175
EWA	0.0949	0.0669	0.1201
EWNA	0.0912	0.0625	0.1145
Matched Filter Freq Domain			
APE	0.1471	0.0644	0.1632
EWA	0.1666	0.0880	0.1927
EWNA	0.1569	0.0876	0.1829
Maximum Likelihood			
APE	0.4677	0.0472	0.4713
EWA	0.4676	0.0472	0.4712
EWNA	0.4676	0.0472	0.4712
Normalized Matched Filter			
APE	0.0921	0.0505	0.1090
EWA	0.1013	0.0620	0.1231
EWNA	0.1038	0.0578	0.1235

5.3.1 Peak Estimator. Similar to the simulation, the peak estimator was applied to waveforms using four different interpolation strategies. In every set of data, some level of interpolation reduced the RMSE. The averaged RMSE for uninterpolated waveforms using the peak estimator in a 121 pixel region was .2053 m and the least RMSE was produced by the spline interpolated waveform at .1608 m, nearly a 4 cm improvement in bias reduction. In the regions of 500 pixels the RMSE was slightly increased for each method, with the uninterpolated waveforms producing an RMSE of .2195 m. The best interpolation method in the 500 pixel region was still the spline method with an increased RMSE of .1755. The lower SNR of the decreased intensity signals could explain for more shifted peaks and greater interpolation error in the interpolated signals when using a larger area of pixels for the range estimation measurements.

The peak estimator methods are exceptionally fast when implemented in Matlab® using a 2.49 GHz processor. Without interpolation, the peak estimator can process 121 pixels in about 0.25 seconds. The peak estimator using spline interpolation is about twice as slow, but still able to process 121 pixels in about .59 seconds. Interpolation makes the algorithm slower than the frequency domain version of the matched filter, but still about 8 times faster than the slowest algorithm, the normalized matched filter. In spite of its speed, the bias in a peak estimator is still in the range of 16-21 cm. The tradeoff in the peak estimator lies in the balance between speed and accuracy. Table 5.8 shows the results of the other algorithms in terms of processing time.

Table 5.8: Algorithm processing times using a computer with a 2.49 GHz processor.

Algorithm	121 pixels (sec)	Full 128 x 128 Array (min)
Peak Estimator (no interp.)	0.0363	0.0819
Peak Estimator (spline interp.)	0.2541	0.5734
Matched Filter Freq. Domain	0.1452	0.3277
Matched Filter Time Domain	1.2015	2.7034
Maximum Likelihood	0.7151	1.6111
Normalized Matched Filter	2.2554	5.0790

5.3.2 Matched Filter. The matched filter was implemented in three different ways. The time domain, frequency domain, and normalized versions each had unique results involving the PWE techniques applied to each algorithm.

5.3.2.1 Time Domain. In contrast to the simulations, the unnormalized matched filter implemented in the time domain experiment proved to yield the most positive results out of all the algorithms in terms of bias on average. There is still a bias in the measurements most likely due to inaccuracies in the reference model and waveforms that are not centered in the range gate. The matched filter in the time domain was able to accurately distinguish ranges within approximately 10 cm when 121 pixels were averaged and within about 6 cm when 500 pixels were used.

The time domain algorithm implementation produced varying results depending on the PWE technique applied. In the 121 pixel trials, the APE algorithm produced the least total error of .1189 m. In the the 500 pixel trials, the EWA algorithm produced the least total error of .1145 m. With a smaller area of pixels, there is less likely a chance for timing jitter or other noises to shift the pulses, so using an averaged waveform to calculate the pulse width produces a lower error. However, in the larger region, it is more sensible to calculate the pulse width for each waveform and then average as there is more likely a chance for the waveforms to shift position.

5.3.2.2 Frequency Domain. The frequency domain matched filter behaved as expected based on the simulated results. It exhibited a large degree of standard deviation among the measurements and showed a large bias in the RMSE. Similar to the time domain implementation, the results of the frequency domain implementation improved by using a larger pixel area. The APE method produced the least total error in both the 121 and 500 pixel regions with values of .2286 m and .1632 m respectively.

5.3.2.3 Normalized. The normalized matched filter had high expectations for removing bias in the range measurements of waveforms that were off center.

However, it did not reduce the RMSE as it did in simulations and did not perform as well as the un-normalized matched filter. The average RMSE of the normalized matched filter was at best .133 m when using the APE algorithm and had a relatively low standard deviation of .0414 m in the 121 pixel data set. When 500 pixels were used in the range estimation the average RMSE dropped about 4 cm to .0921 m with a standard deviation of about .0505 m as seen in Table 5.7. The unexpected poor performance in the measured data is due to the normalized matched filter's sensitivity to inaccuracies in the reference waveform. As shown in the simulations, when the pulse width estimate is off, the normalized matched filter performs about as well as the matched filter in the time domain.

5.3.3 Maximum Likelihood. The maximum likelihood estimator provided the results largest in contrast to the simulated results. Instead of performing comparable to the matched filter implementation, it showed a large degree of total error in measurements. It consistently underestimated the range. Unlike the other range estimation algorithms, the ML estimator did not improve when the number of pixels used in the estimation was increased from 121 to 500. Total error increased about 7 cm from .4016 m in the 121 pixel region to .4713 m in the 500 pixel region. In contrast to the matched filter, the maximum likelihood algorithm does not seem to be affected much by the PWE technique chosen. Referencing Tables 5.6 and 5.7, the ML estimator delivered approximately the same results regardless of the PWE method. The ML estimator appears to be sensitive to changes in the underlying model, but the pulse width estimate used does not have as strong as an effect on the error. As more pixels are used in the range estimate, there is a stronger chance of using pixels that deviate from the original model. It would appear from the results the model itself for the ML estimator (Gaussian wave with Poisson noise) would need refining to improve the estimator.

5.3.4 Clock Cycle Observations in ASC 3-D Flash LADAR Camera. If the average range difference results for each cube of data are plotted in time, then it

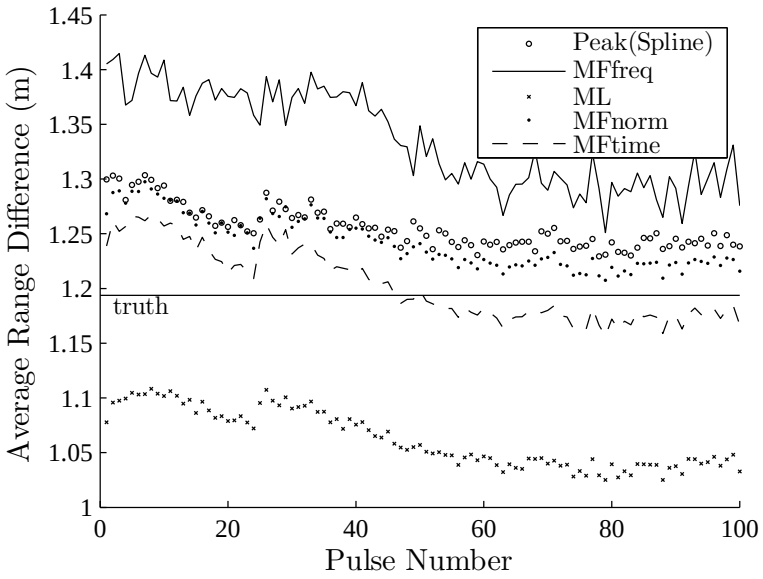

Figure 5.9: Range estimate techniques with respect to clock cycle.

is possible to track the clock cycle of the camera as each laser pulse is fired. The results can provide insight to if there are any other additional noise sources in the camera based on timing or other unknown factors. Figure 5.9 shows the results of one data set when the true range difference was 1.19 meters. The values along the y-axis indicate the average range difference found in each cube of data produced by a return pulse, and the x-axis indicates the pulse or data cube number. As seen in Figure 5.9 there is a fluctuation in values that could be dependent on internal clock of the LADAR system. Figure 5.10 shows the average error (range difference - truth) in each algorithm with respect to the clock cycle. A designed test with more pulses fired would be necessary to determine if the values would stabilize over time or continue to fluctuate.

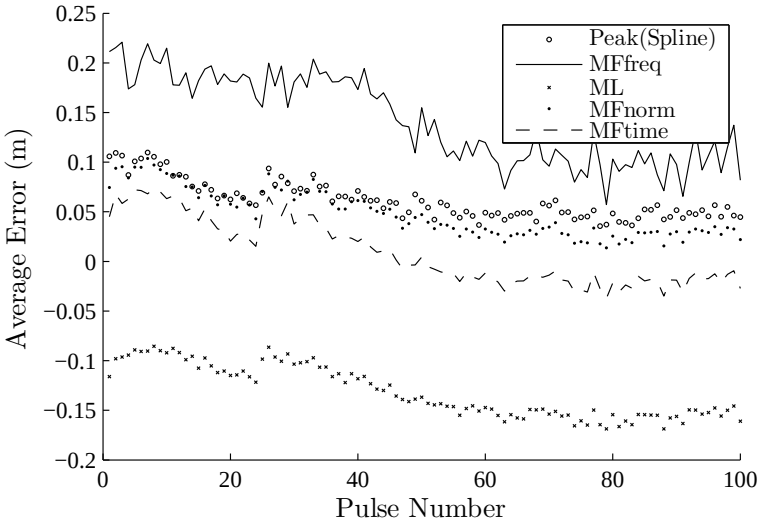

Figure 5.10: Range error with respect to clock cycle.

VI. Conclusion

6.1 Conclusions from Results

Based on the experiments conducted in the scope this research, several key conclusions can be drawn from the results. As observed in other projects involving the ASC 3-D Flash LADAR camera, the noise contained in individual measurements makes absolute range estimates in a single measurement unreliable [7]. Any usable range measurement where the precision is desired to be within several centimeters must be averaged over multiple frames to eliminate the effects of the shot noise.

The peak estimator is a quick and effective tool for estimating ranges provided there are several hundred pixels of information and frames to average over. The peak estimator would probably be best for averaging out the noise to estimate a range to large flat surface target. It would most likely not be able to distinguish features that contained a great deal of detail unless there were numerous frames collected to average over.

The model used for the maximum likelihood estimator is most likely flawed based on the strong bias error shown in the results of the measured data experiment. Based on the simulations, it has been shown to be effective when the model is properly calibrated, but the measured data results show the potential for high error when using the wrong combination of reference wave and noise distribution. In the simulation, the only sources of noise were from simulated background and shot noise. The measured data could possibly also contain a source of Gaussian noise from the electronics involved that was not properly accounted for when designed the maximum likelihood algorithm. Further research could explore which noise type (Poisson versus Gaussian) has the greatest effect on the signal. Because the probability distribution for the waveform and noise will always be somewhat of an estimate, it may never prove to be a reliable source for range estimation.

The matched filters, like the maximum likelihood estimator, show a strong potential for excellent range estimation in simulations. However, their dependence on the accuracy of a reference waveform limit their potential in measured data. While

the normalization technique presented in the research can eliminate the bias produced in partial or uncentered waveforms, it greatly increases the sensitivity of the estimator with respect to its reference waveform. The unnormalized matched filter technique involves less mathematical operations and will therefore perform faster. By not normalizing the waveforms, the estimation technique is vulnerable to a bias error from waveforms that are on the edges of the range gate, but it is not as sensitive to the errors in pulse width estimation. The matched filter implemented in the time domain is a stronger performer in terms of both bias and variance of range measurements when compared to the frequency domain implementation. To account for the speed difference that is often favored by the frequency domain implementation, one could implement look up tables and preprogrammed values for reference waveforms or pulse width estimates.

The choice in algorithm would rely mainly on an application's exact requirements for speed and accuracy. Algorithms such as the peak estimator or frequency domain matched filter display a lower degree of accuracy, but deliver strong performance in the speed category. A time domain implementation of the matched filter may improve range estimation accuracy, but will suffer from increased processing time. The balance in trade off between speed and accuracy will have to ultimately be determined by user requirements.

6.2 Recommendations for Future Research

Several options exist for expanding the research performed during the scope of this thesis. One could spend more time characterizing the pulse shapes produced by the laser in order to form a more robust waveform model. This could be in terms of pulse width shape for use in the matched filters or in terms of probability distribution to use with a maximum likelihood algorithm. Another option could involve finding a faster and more accurate method for estimating the pulse width used for the developing the waveform model. The effects of gain variation have been studied with the older camera model, but it has not yet been documented with the

new camera to verify if any conclusions can be drawn regarding the effects of non linear gain in the pixels of the new camera that was used to collect data for this research. Based on the simulations that show the strong potential of a maximum likelihood estimator with an accurate model, it would be useful to develop other maximum likelihood estimators with different combinations of pulse model and noise distribution to test in a controlled measured data experiment to see which performed the best and which was the most sensitive to changes in pulse width estimation errors. The same process could be implemented to attempt to design a correlation technique that removes the bias like the normalization process, but also minimizes the overall sensitivity to slight changes in the reference model.

Appendix A. Results From Individual Data Sets

A.1 Results from Sular9ft1.SEQ

Table A.1 lists the average RMSE, standard deviation, and total error from Sular9ft1.SEQ when 121 pixels were used in the range measurements.

Table A.1: Results from Sular9ft1.SEQ using 121 pixels to find average range difference.

	Avg RMSE (m)	Avg Std Dev (m)	Avg Total Error (m)
Peak Estimator			
No Interpolation	0.2144	0.0114	0.2147
Linear Interpolation	0.1921	0.0122	0.1925
Spline Interpolation	0.1463	0.0135	0.1469
Pchip Interpolation	0.2365	0.0245	0.2377
Matched Filter Time Domain			
APE	0.0837	0.0242	0.0871
EWA	0.0843	0.0235	0.0875
EWNA	0.0841	0.0229	0.0872
Matched Filter Freq Domain			
APE	0.2403	0.0152	0.2407
EWA	0.2402	0.0149	0.2406
EWNA	0.2394	0.0153	0.2398
Maximum Likelihood			
APE	0.0794	0.0253	0.0833
EWA	0.0792	0.0251	0.0831
EWNA	0.0793	0.0252	0.0832
Normalized Matched Filter			
APE	0.1216	0.0147	0.1225
EWA	0.1194	0.0161	0.1205
EWNA	0.1226	0.0159	0.1236

Table A.2 lists the average RMSE, standard deviation, and total error from Sular9ft1.SEQ when approximately 500 pixels were used in the range measurements.

Table A.2: Results from Sular9ft1.SEQ using approximately 500 pixels to find average range difference.

	Avg RMSE (m)	Avg Std Dev (m)	Avg Total Error (m)
Peak Estimator			
No Interpolation	0.1377	0.0328	0.1415
Linear Interpolation	0.0967	0.0305	0.1014
Spline Interpolation	0.0644	0.0201	0.0675
Pchip Interpolation	0.1344	0.0216	0.1361
Matched Filter Time Domain			
APE	0.0344	0.0330	0.0477
EWA	0.0338	0.0322	0.0467
EWNA	0.0349	0.0317	0.0472
Matched Filter Freq Domain			
APE	0.1486	0.0437	0.1548
EWA	0.1485	0.0449	0.1551
EWNA	0.1423	0.0480	0.1502
Maximum Likelihood			
APE	0.1339	0.0259	0.1363
EWA	0.1337	0.0258	0.1362
EWNA	0.1336	0.0258	0.1361
Normalized Matched Filter			
APE	0.1216	0.0147	0.0588
EWA	0.1194	0.0161	0.0583
EWNA	0.1226	0.0159	0.0634

A.2 Results from Sular9ft2.SEQ

Table A.3 lists the average RMSE, standard deviation, and total error from Sular9ft2.SEQ when 121 pixels were used in the range measurements.

Table A.3: Results from Sular9ft2.SEQ using 121 pixels to find average range difference.

	Avg RMSE (m)	Avg Std Dev (m)	Avg Total Error (m)
Peak Estimator			
No Interpolation	0.2709	0.0403	0.2739
Linear Interpolation	0.2830	0.0288	0.2845
Spline Interpolation	0.1997	0.0232	0.2011
Pchip Interpolation	0.2892	0.0325	0.2910
Matched Filter Time Domain			
APE	0.0312	0.0238	0.0392
EWA	0.0307	0.0230	0.0383
EWNA	0.0309	0.0227	0.0834
Matched Filter Freq Domain			
APE	0.2979	0.0743	0.3070
EWA	0.2986	0.0773	0.3085
EWNA	0.3095	0.0886	0.3219
Maximum Likelihood			
APE	0.1975	0.0230	0.1989
EWA	0.1975	0.0230	0.1989
EWNA	0.1978	0.0232	0.1991
Normalized Matched Filter			
APE	0.1499	0.0151	0.1507
EWA	0.1479	0.0185	0.1491
EWNA	0.1509	0.0190	0.1521

Table A.4 lists the average RMSE, standard deviation, and total error from Sular9ft2.SEQ when approximately 500 pixels were used in the range measurements.

Table A.4: Results from Sular9ft2.SEQ using approximately 500 pixels to find average range difference.

	Avg RMSE (m)	Avg Std Dev (m)	Avg Total Error (m)
Peak Estimator			
No Interpolation	0.1736	0.0351	0.1771
Linear Interpolation	0.1710	0.0178	0.1719
Spline Interpolation	0.1099	0.0270	0.1132
Pchip Interpolation	0.1815	0.0199	0.1826
Matched Filter Time Domain			
APE	0.0625	0.0341	0.0713
EWA	0.0613	0.0331	0.0697
EWNA	0.0579	0.0323	0.0663
Matched Filter Freq Domain			
APE	0.1729	0.0573	0.1822
EWA	0.1734	0.0611	0.1838
EWNA	0.1590	0.0701	0.1738
Maximum Likelihood			
APE	0.2502	0.0224	0.2512
EWA	0.2501	0.0224	0.2511
EWNA	0.2500	0.0224	0.2510
Normalized Matched Filter			
APE	0.0760	0.0253	0.0800
EWA	0.0754	0.0280	0.0804
EWNA	0.0889	0.0246	0.0922

A.3 Results from Sular19ft1.SEQ

Table A.5 lists the average RMSE, standard deviation, and total error from Sular19ft1.SEQ when 121 pixels were used in the range measurements.

Table A.5: Results from Sular19ft1.SEQ using 121 pixels to find average range difference.

	Avg RMSE (m)	Avg Std Dev (m)	Avg Total Error (m)
Peak Estimator			
No Interpolation	0.1126	0.0594	0.1273
Linear Interpolation	0.0967	0.0278	0.1006
Spline Interpolation	0.0919	0.0130	0.0929
Pchip Interpolation	0.0938	0.0388	0.1015
Matched Filter Time Domain			
APE	0.0895	0.0159	0.0910
EWA	0.0879	0.0160	0.0894
EWNA	0.0876	0.0160	0.0890
Matched Filter Freq Domain			
APE	0.1516	0.0706	0.1672
EWA	0.1458	0.0741	0.1635
EWNA	0.1413	0.0757	0.1602
Maximum Likelihood			
APE	0.7152	0.0149	0.7154
EWA	0.7150	0.0149	0.7151
EWNA	0.7150	0.0150	0.7151
Normalized Matched Filter			
APE	0.0896	0.0159	0.0910
EWA	0.0880	0.0160	0.0894
EWNA	0.0875	0.0160	0.0889

Table A.6 lists the average RMSE, standard deviation, and total error from Sular19ft1.SEQ when approximately 500 pixels were used in the range measurements.

Table A.6: Results from Sular19ft1.SEQ using approximately 500 pixels to find average range difference.

	Avg RMSE (m)	Avg Std Dev (m)	Avg Total Error (m)
Peak Estimator			
No Interpolation	0.1493	0.0549	0.1590
Linear Interpolation	0.1232	0.0283	0.1264
Spline Interpolation	0.1173	0.0042	0.1174
Pchip Interpolation	0.1251	0.0385	0.1308
Matched Filter Time Domain			
APE	0.0885	0.0090	0.0900
EWA	0.0876	0.0090	0.0880
EWNA	0.0900	0.0090	0.0903
Matched Filter Freq Domain			
APE	0.1664	0.0609	0.1772
EWA	0.1626	0.0650	0.1752
EWNA	0.1608	0.0684	0.1747
Maximum Likelihood			
APE	0.7738	0.0156	0.7740
EWA	0.7735	0.0157	0.7737
EWNA	0.7736	0.0157	0.7738
Normalized Matched Filter			
APE	0.0886	0.0089	0.0890
EWA	0.0876	0.0089	0.0880
EWNA	0.0898	0.0089	0.0903

A.4 Results from Sular19ft2.SEQ

Table A.7 lists the average RMSE, standard deviation, and total error from Sular19ft2.SEQ when 121 pixels were used in the range measurements.

Table A.7: Results from Sular19ft2.SEQ using 121 pixels to find average range difference.

	Avg RMSE (m)	Avg Std Dev (m)	Avg Total Error (m)
Peak Estimator			
No Interpolation	0.2235	0.1588	0.2742
Linear Interpolation	0.1914	0.1348	0.2341
Spline Interpolation	0.2053	0.1371	0.2470
Pchip Interpolation	0.1983	0.1447	0.2455
Matched Filter Time Domain			
APE	0.2000	0.1634	0.2583
EWA	0.2231	0.1936	0.2954
EWNA	0.2076	0.1743	0.2711
Matched Filter Freq Domain			
APE	0.1678	0.1081	0.1996
EWA	0.2167	0.1810	0.2823
EWNA	0.2012	0.1594	0.2567
Maximum Likelihood			
APE	0.5943	0.1330	0.6090
EWA	0.5944	0.1335	0.6092
EWNA	0.5944	0.1333	0.6093
Normalized Matched Filter			
APE	0.1708	0.1197	0.2086
EWA	0.2179	0.1858	0.2864
EWNA	0.1983	0.1604	0.2551

Table A.8 lists the average RMSE, standard deviation, and total error from Sular19ft2.SEQ when approximately 500 pixels were used in the range measurements.

Table A.8: Results from Sular19ft2.SEQ using approximately 500 pixels to find average range difference.

	Avg RMSE (m)	Avg Std Dev (m)	Avg Total Error (m)
Peak Estimator			
No Interpolation	0.4173	0.0934	0.4276
Linear Interpolation	0.4157	0.0876	0.4249
Spline Interpolation	0.4104	0.0820	0.4185
Pchip Interpolation	0.4143	0.0883	0.4236
Matched Filter Time Domain			
APE	0.1874	0.1833	0.2621
EWA	0.1971	0.1935	0.2762
EWNA	0.1821	0.1772	0.2541
Matched Filter Freq Domain			
APE	0.1004	0.0957	0.1387
EWA	0.1819	0.1809	0.2566
EWNA	0.1653	0.1639	0.2328
Maximum Likelihood			
APE	0.7129	0.1248	0.7237
EWA	0.7129	0.1249	0.7238
EWNA	0.7129	0.1247	0.7238
Normalized Matched Filter			
APE	0.1503	0.1436	0.2079
EWA	0.1899	0.1858	0.2657
EWNA	0.1783	0.1728	0.2483

Bibliography

1. Burris, Charles R. *An Estimation Theory Approach to Detection and Ranging of Obscured Targets in 3-D LADAR Data*. Master's thesis, Graduate School of Engineering, Air Force Institute of Technology (AETC), Wright-Patterson AFB OH, March 2006. AFIT/GE/ENG/06-10.

2. Cain, Stephen, Richard Richmond, and Ernest Armstrong. "Flash light detection and range accuracy limits for returns from single opaque surfaces via Cramer-Rao bounds". *Applied Optics*, 45(24):46–56, August 2006.

3. Gelbart, Asher, Chris Weber, Shannon Bybee-Driscoll, Jonathan Freeman, Gregory J. Fetzer, Tom Seales, Karen A. McCarley, and Jim Wright. "FLASH lidar data collections in terrestrial and ocean environments". *Proceedings of SPIE - The International Society for Optical Engineering*, 5086:27–38, April 2003.

4. Gonzalez, R.C. and R.E. Woods. *Digital Image Processing*. Prentice-Hall, Upper Saddle River, New Jersey, second edition, 2002.

5. Goodman, Joseph W. *Statistical Optics*. John Wiley and Sons, New York City, New York, first edition, 1985.

6. Jelalian, Albert V. *Laser Radar Systems*. Artech House, Boston, Massachusetts, first edition, 1992.

7. Johnson, Steven and Stephen Cain. "Gain Variation and Gain Equalization in Arrays of Avalanche Photodiodes", 2008.

8. Lewis, J.P. "Fast Template Matching". *Vision Interface*, 120–123, 1995.

9. Pletta, J. Bryan and John Sackos. *An advanced unmanned vehicle for remote applications*. Technical report, Sandia National Laboratories, March 1998.

10. Sackos, John, Bart Bradley, Bob Nellums, and Carl Diegert. "The emerging versatility of a scannerless range imager". *SPIE International Symposium on Aerospace/Defense Sensing and Controls*.

11. Seal, Michael D. *Nonlinear Time-Variant Response in an Avalanche Photodiode Array Based Laser Detection and Ranging System*. Master's thesis, Graduate School of Engineering, Air Force Institute of Technology (AETC), Wright-Patterson AFB OH, March 2007. AFIT/GEO/ENG/07-03.

12. Seidel, Christian, Ingo Schwartz, and Peter Kielhorn. "Helicopter collision avoidance and brown-out recovery with HELLAS". *Proceedings of SPIE - The International Society for Optical Engineering*, 7114:27–38, September 2008.

13. Stettner, Roger, Howard Bailey, and Richard Richmond. "Eye-Safe Laser Radar 3-D Imaging". *Proceedings of SPIE - The International Society for Optical Engineering*, 4377:46–56, April 2001.

REPORT DOCUMENTATION PAGE

Form Approved
OMB No. 0704-0188

1. REPORT DATE *(DD-MM-YYYY)*	2. REPORT TYPE	3. DATES COVERED *(From - To)*
26-03-2009	Master's Thesis	May 2007 - March 2009

4. TITLE AND SUBTITLE
Range Estimation Algorithm Comparison in 3-D Flash LADAR Data

5a. CONTRACT NUMBER

5b. GRANT NUMBER

5c. PROGRAM ELEMENT NUMBER

6. AUTHOR(S)
Jordan, Steven P, Captain, USAF

5d. PROJECT NUMBER
JON ENG09-128

5e. TASK NUMBER

5f. WORK UNIT NUMBER

7. PERFORMING ORGANIZATION NAME(S) AND ADDRESS(ES)
Air Force Institute of Technology
Graduate School of Engineering and Management (AFIT/EN)
2950 Hobson Way, Building 640
WPAFB OH 45433-8865

8. PERFORMING ORGANIZATION REPORT NUMBER
AFIT/GE/ENG/09-22

9. SPONSORING/MONITORING AGENCY NAME(S) AND ADDRESS(ES)
Jack Woods
Air Force Research Lab Sensors Directorate
Electro-Optics Combat ID Technology Branch
2241 Avionics Circle, Bldg 622, Wright-Patterson AFB OH 45433
DSN: 785-9614 Email: jack.woods@wpafb.af.mil

10. SPONSOR/MONITOR'S ACRONYM(S)
AFRL/RYJM

11. SPONSOR/MONITOR'S REPORT NUMBER(S)

12. DISTRIBUTION/AVAILABILITY STATEMENT

13. SUPPLEMENTARY NOTES

14. ABSTRACT

Peak, maximum likelihood (ML), and matched filter (MF) range estimation algorithms were tested in both simulated and measured 3-D Flash LADAR data. A normalized version of the MF was also developed and tested. Three different methods based on averaging were developed to calibrate the pulse width of the reference waveform used in the MF and ML algorithms. Simulation results show that a MF produces a bias when waveforms are cropped or shifted off center within a range gate, but normalizing waveforms before computing the cross correlation can reduce the average bias. The ML algorithm also produces a bias in shifted waveforms based on their position within the range gate. The peak estimator suffers from high variance in measurements due to the effect of shot noise on waveforms. In the measured data sets, normalization did not reduce the bias in MF results because it increased the algorithm's sensitivity to errors in the reference waveform. The ML estimator resulted in the largest bias in the results and was attributed to an underlying flaw in the probability model based on a Gaussian waveform with Poisson noise.

15. SUBJECT TERMS
Flash LADAR, laser detection and ranging, range estimation algorithms

16. SECURITY CLASSIFICATION OF:			17. LIMITATION OF ABSTRACT	18. NUMBER OF PAGES	19a. NAME OF RESPONSIBLE PERSON
a. REPORT	b. ABSTRACT	c. THIS PAGE			Dr. Stephen C. Cain
U	U	U	UU	102	19b. TELEPHONE NUMBER *(Include area code)* (937) 255-3636 x4617 stephen.cain@afit.edu